KONINKLIJK NEDERLANDS METEOROLOGISCH INSTITUUT

MEDEDELINGEN EN VERHANDELINGEN

No. 74

Dr. H. M. DE JONG

GEOSTROPHIC FLOW

GEOSTROPHIC APPROXIMATION IN THE UPPER AIR FLOW WITH APPLICATION TO AERONAVIGATION AND AIR TRAJECTORIES

1959

F 5,00

STAATSDRUKKERIJ- EN UITGEVERIJBEDRIJF / 'S-GRAVENHAGE

GEOSTROPHIC FLOW

GEOSTROPHIC APPROXIMATION IN THE UPPER AIR FLOW

WITH APPLICATION TO AERONAVIGATION AND AIR TRAJECTORIES

KONINKLIJK
NEDERLANDS METEOROLOGISCH INSTITUUT

MEDEDELINGEN EN VERHANDELINGEN

No. 74

Dr. H. M. DE JONG

GEOSTROPHIC FLOW

GEOSTROPHIC APPROXIMATION IN THE UPPER AIR FLOW WITH APPLICATION TO AERONAVIGATION AND AIR TRAJECTORIES

1959

STAATSDRUKKERIJ- EN UITGEVERIJBEDRIJF / 's-GRAVENHAGE

PUBLICATIENUMMER: K.N.M.I. 102-74

U.D.C.: 551.501.7:
551.511.2:
551.557:
629.13

PREFACE

The expansion of commercial air traffic by operations with turbine powered aircraft gives rise to new problems in meteorological research in the higher levels of the atmosphere. Especially those items which are closely related to altimetry, flight planning, drift determination and aeronavigation should be re-examined in the scope of the flight characteristics of this new type of aircraft.

Participating in a special commission established in order to consider the briefing of long range flights with turbine powered aircraft, the author made a study of these problems, the results of which are presented in this paper.

Dr. F. H. Schmidt, the chairman of the commission, contributed to this publication by many discussions with the author and critical reading of the manuscript; Dr. J. L. Spier prepared the upper air charts.

The Director in chief
of the
Royal Netherlands Meteorological Institute.
IR. C. J. WARNERS

CONTENTS

INTRODUCTION

In synoptic and aeronautical meteorology the upper air flow plays a dominant part in daily work and theoretical investigations. The structure and development of the motion is concealed in the hydrodynamic and thermodynamic equations but in virtue of their complexity these equations are far from being accessible for a complete analytical description. For practical reasons one is therefore forced to simplify the basic equations in order to arrive at a fairly good approximation of the air motion. One of these simplifications involves the elimination of accelerations and vertical motions of the air, resulting in the well-known geostrophic wind equation. The approximation of the air flow which is actually based on this geostrophic wind equation is applied successfully when dealing with activities which in the first instance demand rough treatment of the subjects. In this respect it may be pointed out that several ideas and objectives in practical meteorology make use of this geostrophic wind approximation. Especially in aeronavigation and altimetry it is the basic tool for different methods of procedure. It was partly owing to the stimulus of some unsolved questions there, that this paper was written. The most important questions involve the modification of some pressure pattern techniques for turbo prop and turbo jet aircraft and the precise meaning of composite charts. The discussion of these problems starts with a general investigation in terms of time and height dependent geostrophic flow. (parts I, II and III). In part IV the results obtained therefrom are applied with respect to some aspects of aeronavigation especially as regards those for turbine aircraft. Finally in part V a more or less academic problem has been worked out concerning trajectories of air particles within specified velocity fields.

PART I

PHYSICAL SURFACES IN THE ATMOSPHERE WITH GEOSTROPHIC FLOW

The well-known geostrophic wind equation in isobaric surfaces is considered to give a fairly good approximation of the velocity field in the earth's atmosphere. The horizontal projection of the isobaric windfield may be interpreted as a two-dimensional velocity field with stream function. Since the geostrophic approximation may be assumed for any pressure surface and pressure may serve as the vertical coordinate in the atmosphere, the problem arises whether the (horizontal projection of the) windfield in an arbitrary surface may still be conceived as a velocity field with stream function. It has already been shown by Montgomery [1937] that this is true for the isentropic surfaces. In this part it will be demonstrated that apart from the isobaric and isentropic surface there exists a whole family of physical surfaces in the atmosphere with the property quoted above.

1. Geostrophic flow

In the free atmosphere the velocity field of large scale motions permits us to define a *geostrophic* wind velocity in every point of a horizontal surface.

If $\mathbf{k}$ denotes the unit vector pointing to local zenith, z represents height above sea level, p pressure, ρ density and

$$\lambda = 2\,\Omega \sin L$$

the vertical component of the angular velocity $2\,\boldsymbol{\Omega}$ of earth's rotation at latitude L (Coriolis parameter), then the geostrophic equation may be written in vector form

$$\mathbf{v}_g = \mathbf{k} \wedge \frac{1}{\lambda\rho}\, \nabla_z\, p. \tag{I.1}$$

Here bold characters denote vectors, the subscript z refers to the usual gradient operator in a horizontal surface.

The equation assumes a simpler form when pressure is used as a vertical coordinate instead of height.

Applying the *hydrostatic equation,* (g acceleration of gravity),

$$\frac{\delta p}{\delta z} = -g\rho, \tag{I.2}$$

which expresses that the force of gravity is balanced by the vertical pressure force, we obtain the modified geostrophic equation

$$\mathbf{v}_g = \mathbf{k} \wedge \frac{g}{\lambda} \nabla_p z,$$

where the subscript p now indicates the horizontal gradient operator in a horizontal projection of the isobaric surface.

Introducing the concept of *geopotential* φ, or *gravity potential*

$$d\varphi = gdz, \tag{I.3}$$

equation (I.1) takes the form

$$\mathbf{v}_g = \mathbf{k} \wedge \frac{1}{\lambda} \nabla_p \varphi. \tag{I.4}$$

As the unit of geopotential the standard geopotential meter (gpm) has been adopted, defined by

$$1 \text{ gpm} = 9{,}80665 \text{ m}^2 \text{ sec}^{-2}.$$

In the lower atmosphere, where g is about 980 cm.sec.$^{-2}$ the geometric height in meters and geopotential in geopotential meters are approximately equal.

The geostrophic windvector is directed along the isobars in a horizontal surface or along the contour lines of an isobaric surface. Pure geostrophic winds exist in frictionless adiabatic motions, if the earth's curvature is neglected and the Coriolis parameter is regarded as constant. The accelerations vanish and the horizontal pressure force is balanced by the Coriolis force. The *geostrophic flow* associated with it represents a steady flow along parallel, straight horizontal streamlines.

In large scale motions in middle and high latitudes, however, the accelerations are usually so small that the geostrophic departure is considerably smaller than the wind itself. As a consequence the geostrophic wind can be used as a first approximation for the wind velocity.

Whether the approximation is an accurate one is difficult to prove. The geostrophic departures found by comparing rawins and contour-measured winds, as such, include all errors of analysis, map reading and wind measurement. The justification of the wind approximation therefore depends on the evaluation of the *apparent* ageostrophic deviations. For spot winds over the British Isles Murray [1954] derived apparent ageostrophic root mean square vector deviations at 500, 300 and 200 mb as 14, 20 and 18 kn, showing that the deviations increase from the 500 mb level, which is in the vicinity of the level of non-divergence, upwards to the higher levels of the troposphere. Kochansky [1958] found at 200 and 300 mb approximately 16 kn. These figures should be interpreted with some caution, since the uncertainty in the wind observation increases considerably with height. Due to the short period time- and space variability of the wind, and observational errors, the profiles of observed winds often show phenomenal fluctuations already above 7 km, Reiter [1958]. At the same time the uncertainty in the contour spacing increases, caused by the increasing errors in the geodynamic height, computed from radio soundings. Thus until better means of measuring wind and geopotential are developed, geostrophic winds can be considered a workable proposition. That is the reason why the geostrophic approximation is extensively used in synoptic as well as in aeronautical meteorology and is also applied in theoretical investigations. In this publication the approximation is assumed to be justified at any pressure level and to be valid at any time.

By its simple form a number of devices have been designed to measure wind speed and direction from upper air charts using the geostrophic relationship, and geostrophic altimetry is mainly based on the concept of geostrophic winds.

Montgomery [1937] has shown that the geostrophic wind in isentropic surfaces takes the form

$$\mathbf{v}_g = \mathbf{k} \wedge \frac{1}{\lambda} \nabla_\theta \psi_M, \tag{I.5}$$

where Θ refers to the potential temperature and ψ_M represents the *isentropic stream function* or *Montgomery's acceleration potential*

$$\psi_M = \varphi + c_p T, \tag{I.6}$$

φ representing the geopotential of the isentropic surface, c_p the specific heat at constant pressure and T temperature.

The geostrophic windvector on isentropic surfaces is directed along the curves $\psi_M =$ constant. Equation (I.5) is used in isentropic analyses.

At this point one may put the question whether the geostropic flow concept is valid in isobaric and isentropic surfaces only?

The answer to this question is given in the next section. As a result a whole set of physical surfaces with geostrophic flow is found, including isothermal and isosteric surfaces.

2. Surfaces with geostrophic flow

Neglecting the variability of the Coriolis parameter the geostrophic equation in isobaric surfaces may be written

$$\mathbf{v}_g = -\mathbf{k} \wedge \nabla \xi = \mathbf{k} \wedge \frac{1}{\lambda} \nabla_p \varphi,$$

where the function $\xi = -\dfrac{\varphi}{\lambda}$ plays the rôle of a *stream function.* The geostrophic approximation is valid in every isobaric surface. Therefore the geopotential depends not only on the east-west and north-south components x and y, but involves an additional pressure variable p.

In order to investigate geostrophic flow within specified surfaces, we introduce an arbitrary "space function" $p = p(x, y)$, continuous and differentiable with respect to x and y.

If $(\quad)_p$ means a substitution for the space function p(x, y) in the expression in brackets, then the wind in a horizontal projection of the arbitrary surface s may be written

$$\mathbf{v}_s = -\mathbf{k} \wedge (\nabla \xi)_p.$$

When $\nabla \xi$ is split up into its components, we derive, after partial differentiation with respect to x and y, for composed functions,

$$(\nabla \xi)_p = \nabla(\xi)_p - \left(\frac{\partial \xi}{\partial p}\right)_p \nabla p$$

Hence we may write

$$\mathbf{v}_s = -\mathbf{k} \wedge \nabla(\xi)_p + \mathbf{k} \wedge \left(\frac{\partial \xi}{\partial p}\right)_p \nabla p \tag{I.7}$$

The first term on the right refers to a gradient vector for the composed stream function $(\xi)_p = \xi(x, y, p(x, y))$, the second to a pressure gradient in the horizontal projection of the surface pressure distribution.

In general the vector configuration $\mathbf{v}_s$ itself cannot be derived from a stream function. Consequently it should be represented graphically by sets of curves, points etc. like isogonals, isotachs, points and lines of convergence and divergence, neutral points and so on. However, we are rather interested in the geostrophic approximation considered in the previous section.

In order for a motion $\mathbf{v}_s$ to possess a stream function it must be non-divergent. Hence, with (I.7)

$$\nabla \cdot \mathbf{v}_s = -\nabla \cdot (\mathbf{k} \wedge \nabla(\xi)_p) + \nabla \cdot (\mathbf{k} \wedge \left(\frac{\partial \xi}{\partial p}\right)_p \nabla p) = 0.$$

According to the vector products

$$\nabla \cdot \left(\mathbf{k} \wedge \nabla(\xi)_p\right) = \nabla(\xi)_p \cdot \left(\nabla \wedge \mathbf{k}\right) - \mathbf{k} \cdot \left(\nabla \wedge \nabla(\xi)_p\right),$$

$$\nabla \cdot \left(\mathbf{k} \wedge \left(\frac{\partial \xi}{\partial p}\right)_p \nabla p\right) = \left(\frac{\partial \xi}{\partial p}\right)_p \nabla p \cdot \left(\nabla \wedge \mathbf{k}\right) - \mathbf{k} \cdot \left(\nabla \wedge \left(\frac{\partial \xi}{\partial p}\right)_p \nabla p\right)$$

and on account of the identity

$$\nabla \wedge \nabla(\xi)_p \equiv 0$$

and

$$\nabla \wedge \mathbf{k} = 0$$

we get

$$\nabla \cdot \mathbf{v}_s = -\mathbf{k} \cdot \left(\nabla \wedge \left(\frac{\partial \xi}{\partial p}\right)_p \nabla p\right) = 0.$$

Besides we have

$$\nabla \wedge \left(\frac{\partial \xi}{\partial p}\right)_p \nabla p = -\nabla p \wedge \nabla \left(\frac{\partial \xi}{\partial p}\right)_p .$$

Thus,

$$\mathbf{k} \cdot \nabla p \wedge \nabla \left(\frac{\partial \xi}{\partial p}\right)_p = 0, \tag{I.8}$$

which expresses that the space function p(x, y) must satisfy the homogeneous partial differential equation

$$\xi_{py}\,\frac{\partial p}{\partial x} - \xi_{px}\,\frac{\partial p}{\partial y} = 0. \tag{I.9}$$

Since the term on the left of (I.8) involves a unit vector and two gradient vectors, the resulting triple scalar product may be expressed in the form

$$J\left(p, \frac{\partial \xi}{\partial p}\right) = 0,$$

where J denotes the Jacobian determinant in the horizontal plane

$$J\left(p, \frac{\partial \xi}{\partial p}\right) = \frac{\partial}{\partial(x, y)}\left(p, \frac{\partial \xi}{\partial p}\right).$$

As a result we find that the horizontal projection of the motion on the surface s, defined by the space function $p = p(x, y)$ behaves like geostrophic flow if the space function is such, that the Jacobian determinant of p and $\frac{\partial \xi}{\partial p}$ vanishes.

With $\xi = -\frac{\varphi}{\lambda}$ the relation with the Jacobian determinant takes the form

$$J\left(p, \frac{\partial \varphi}{\partial p}\right) = 0. \tag{I.10}$$

Now according to the hydrostatic equation (I.2) and equation (I.3) we have

$$\frac{\partial \varphi}{\partial p} = -\frac{1}{\rho}. \tag{I.11}$$

We may therefore write for (I.10)

$$J(p, \rho) = 0.$$

In dry air, the pressure p, absolute temperature T and density ρ fulfill the gas equation

$$p = \rho R T, \tag{I.12}$$

where $R = 2\,87.04 \times 10^6\ m^2 sec^{-2}$ per degree absolute is the gas constant.

In case of moist air *virtual* temperature should be read instead of temperature. Then, with the above equation of state in mind (I.10) becomes

$$J(p, \rho) = J(p, T) = J(\rho, T) = 0. \tag{I.13}$$

These expressions mean geometrically that the surfaces with geostrophic flow intersect the isobaric surfaces along isotherms and in virtue of the gas equation along the isosteric lines. Put otherwise, in surfaces with geostrophic flow the isobars, isotherms and isosteric lines coincide.

To specify these surfaces mathematically we may observe that in the atmosphere any surface may be interpreted to be a scalar surface for a quantity that depends on three parameters, e.g. pressure, (virtual) temperature and height above sea level. Then within the scope of the above result the surfaces with geostrophic flow may be represented by scalar surfaces for scalar functions S which depend on pressure and temperature only or in view of the gas equation, depend on pressure and density, respectively temperature and density only.

We may remark that the coinciding surface isobars, isotherms and isosteric lines happen to be the *characteristic curves* of the partial differential equations (I.13). This may be seen for instance from the equation

$$J(p, T) = 0$$

or

$$T_y \frac{\partial p}{\partial x} - T_x \frac{\partial p}{\partial y} = 0.$$

The characteristic curves are determined by the Lagrange's equations

$$\frac{dx}{d\tau} = T_y$$

$$\frac{dy}{d\tau} = -T_x$$

$$\frac{dp}{d\tau} = 0$$

where τ is any suitable parameter.

In view of this system of equations the characteristic curves are isotherms, embedded in isobaric surfaces. Then, in addition, from the gas equation it follows that the characteristic curves, which generate the scalar surfaces $S =$ constant are coinciding isobars, isotherms and isosteric lines.

Examples of physical surfaces with geostrophic flow are *isothermal surfaces*

$S = T =$ constant, *isosteric surfaces* $S = \rho =$ constant, *isobaric surfaces* $S = p =$ constant and *isentropic surfaces* $S = \Theta =$ constant. The last example in virtue of the definition of potential temperature

$$\Theta = T \left(\frac{1000}{p}\right)^{\frac{R}{c_p}} \tag{I.14}$$

where $\frac{R}{c_p} = 0{,}28$ for dry air is assumed to be constant.

The geostrophic equations for the wind approximation in isobaric and isentropic surfaces are already known, cf. equations (I.4) and (I.5).

In order to evaluate the corresponding equations for every surface with geostrophic flow we return to the equation (I.7).

Substituting for $\xi = -\frac{\varphi}{\lambda}$ and the hydrostatic equation (I.11) the wind vector on an arbitrary surface s takes the form

$$\mathbf{v}_s = \mathbf{k} \wedge \frac{1}{\lambda} \nabla_s \varphi + \mathbf{k} \wedge \frac{1}{\lambda\rho} \nabla_s p, \tag{I.15}$$

showing that the wind is a combination of the expressions (I.1) and (I.4). The first term rcfers to the horizontal gradient of the geopotential of the surface and the second term to the pressure gradient in the horizontal projection of the surface pressure distribution.

Next, let us suppose that s is a scalar surface with geostrophic flow. Then according to the above result the scalar function S should depend only on any two of the three quantities pressure, (virtual) temperature and density, for instance

$$S = S_o = S(p, \rho),$$

which may be rewritten:

$$\rho = \rho(p, S_o).$$

Hence, from equation (I.15) we obtain

$$\mathbf{v}_g = \mathbf{v}_s = \mathbf{k} \wedge \frac{1}{\lambda} \nabla_{s_o} \varphi + \mathbf{k} \wedge \frac{1}{\lambda\rho(p, S_o)} \nabla_{s_o} p$$

$$= \mathbf{k} \wedge \frac{1}{\lambda} \nabla_{S_o} \varphi + \mathbf{k} \wedge \frac{1}{\lambda} \nabla_{S_o} \int_{p_r}^{p} \frac{dp}{\rho(p, S_o)},$$

where p_r refers to an arbitrary reference pressure level. Thus we have

$$\mathbf{v}_g = \mathbf{k} \wedge \frac{1}{\lambda} \nabla_{S_o} \left(\varphi - \varphi_{S_o}\right). \tag{I.16}$$

On account of the hydrostatic equation (I.11) the quantity

$$\varphi_{S_o} = - \int_{p_r}^{p} \frac{dp}{\rho(p, S_o)} \tag{I.17}$$

is to be interpreted as the geopotential of the pressure level p with respect to a reference pressure level p_r in a *barotropic* atmosphere in which the quantity S is constant and equal to S_o.

(I.16) may be written

$$\mathbf{v}_g = \mathbf{k} \wedge \frac{1}{\lambda} \nabla \psi \tag{I.18}$$

where

$$\psi = \varphi - \varphi_{S_o}.$$

We may put $\varphi = gz$, where z denotes true height measured by means of a radio-radar altimeter and $\varphi_{S0} = gz_{S0}$, where z_{S0} indicates a "pressure altitude" which may be measured by a pressure altimeter, provided that it has been calibrated not according to the standard atmosphere, as is usual, but according to the barotropic atmosphere $S = S_o$, then

$$\psi = g(z - z_{S0}) = gD^*$$

and

$$\mathbf{v}_g = \mathbf{k} \wedge \kappa \nabla D^*,$$

$$\kappa = \frac{g}{\lambda}.$$

D^* denotes the difference of readings of both altimeters. If D^* is measured in feet, then

$$\mathbf{v}_g = \frac{21.47}{\sin L_m} \mathbf{k} \wedge \nabla D^*$$

in knots.

When the arbitrary surface happens to be a surface within which the temperature-pressure distribution corresponds to that in the standard atmosphere, then D* reduces to the well-known D-value, which is commonly used in geostrophic altimetry (cf. part IV).

Then the wind equation assumes the form

$$\mathbf{v}_g = \mathbf{k} \wedge \kappa \nabla D. \tag{I.19}$$

Summarizing our results we have:

Applying the geostrophic approximation for the wind distribution in real (baroclinic) atmosphere, the surfaces with geostrophic flow consist of scalar surfaces, for which the scalar function S depends only on any two of the three quantities pressure, density and (virtual) temperature. The geostrophic equation takes the form

$$\mathbf{v}_g = \mathbf{k} \wedge \frac{1}{\lambda} \nabla \psi$$

where ψ denotes the difference between the geopotential φ of the surface with respect to a horizontal level and φ_{s_0} the geopotential of the surface with respect to a fixed reference pressure level in the barotropic atmosphere, defined by $S = S_0 =$ constant.

The surfaces with geostrophic flow are generated by coincident isobars, isotherms and isosteric lines.

In barotropic atmospheres themselves *any* surface will have geostrophic flow and the geostrophic equation simply reduces to the wind equation *in* isobaric surfaces. This may be understood by the remark that in barotropic atmospheres the geostrophic flow is independent of pressure. In expression (I.18) ψ equals the geopotential of the reference pressure level with respect to a horizontal reference level, so that the equation reduces to the form

$$\mathbf{v}_g = \mathbf{k} \wedge \frac{1}{\lambda} \nabla_p \varphi$$

From this result we may conclude that the wind patterns in surfaces with geostrophic flow will differ in appearance, provided that the real atmosphere diverges appreciably from a barotropic atmosphere, in other words when the real atmosphere be baroclinic.

In practice the representation of the air motion takes place by means of drawing isopleths of the stream function, because these isopleths may be interpreted as streamlines of the motion.

In isobaric surfaces for instance this object is gained by the geopotential or contour lines $\varphi =$ const. (Chart 1).

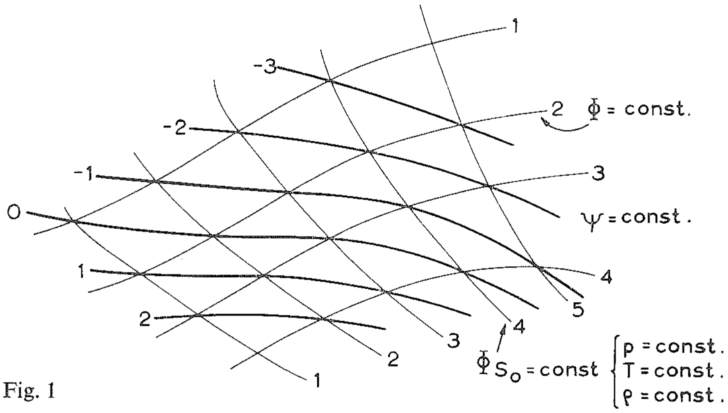

Fig. 1

In the case of an arbitrary surface with geostrophic flow the isopleths consist of lines ψ = constant. Here it is obvious that we perform a graphical subtraction in two patterns, i.e. the set of geopotential- or surface contour lines φ = const. and the set of lines φ_{S_0} = const., or in virtue of the definition of φ_{S_0}, formula (I.17), the set of horizontal projections of the surface isobars (fig. 1). In order to apply the subtraction graphically it is necessary to normalize both scalar patterns, which means that both quantities φ and φ_{S_0} should indicate the same unit of measure and the increment in the φ-pattern be equal to the increment in the φ_{S_0}-pattern. By subtracting the two scalar patterns graphically their gradient patterns are subtracted vectorially, resulting in the representation of the geostrophic approximation of the surface wind flow. The above subtraction method, due to Maxwell, has its counterpart in the graphical addition method, which we shall often have to deal with in later sections.

3. Geostrophic flow in polytropic surfaces

In order to apply the above results on isothermal and isosteric surfaces the geostrophic flow for a wider class of surfaces is investigated.

In dynamic meteorology certain distributions of pressure, temperature and density, compatible with the hydrostatic equation and the gas equation, have been extensively used as model atmospheres. One of these models concerns the *polytropic* atmospheres, which are characterized by a constant lapse rate m of the temperature

$$T = T_0 - mz,$$

where T_0 denotes the temperature at $z = 0$.

The corresponding distribution of pressure and density is

$$\frac{p}{p_o} = \left(\frac{\rho}{\rho_o}\right)^k, \tag{I.20}$$

where
$$k = \frac{g}{g - Rm},$$

$$R = c_p - c_v,$$

c_v being the specific heat at constant volume.

These distributions represent polytropic distributions of class k. The *isothermal atmosphere* is obtained as a special case by taking $m = 0 (k = 1)$. When $m = \frac{g}{c_p}$, $k = \frac{c_p}{c_v}$, the potential temperature is constant. The model atmosphere is then an "*isentropic*" *atmosphere*. Another polytropic model atmosphere is the *homogeneous* or rather *equidense atmosphere*, obtained when $m = \frac{g}{R}$ $(k = \infty)$.

In the real atmosphere, surfaces exist upon which the above defined pressure- and density distribution occur. It is therefore logical to introduce the concept of *polytropic surfaces* of class k, being scalar surfaces for which the scalar function S is defined by

$$S = p\rho^{-k}. \tag{I.21}$$

A polytropic surface of class $k = 0$ refers to a *pressure surface*, that of class $k = 1$ to an *isothermal surface*, that of class $k = \frac{c_p}{c_v}$ to an *isentropic surface* and that of class $k = \infty$ to an *isosteric surface.*

The geostrophic wind equation for polytropic surfaces becomes according to equation (I.16)

$$\mathbf{v}_g = \mathbf{k} \wedge \frac{1}{\lambda} \underset{\text{pol. surf.}}{\nabla} (\varphi - \varphi_{\text{pol.surf.}}), \tag{I.22}$$

where $\varphi_{\text{pol.surf.}}$ represents the geopotential of the polytropic surface with respect to a reference pressure level in a corresponding polytropic model atmosphere.

In order to evaluate $\varphi_{\text{pol.surf.}}$ we evaluate the integral (I.17)

$$\varphi_{\text{pol.surf.}} = - \int_{p_r}^{p} \frac{dp}{\rho(p, S_o)}.$$

In view of (I.21) we have

$$\rho = \left(\frac{p}{S_o}\right)^{\frac{1}{k}}.$$

When this expression is substituted in the integrand we obtain

$$\varphi_{\text{pol.surf.}} = - \int_{p_r}^{p} \left(\frac{p}{S_o}\right)^{-\frac{1}{k}} dp.$$

Integrating for $k \neq 1$, we get

$$\varphi_{\text{pol.surf.}} = \frac{k}{1-k} S_o^{\frac{1}{k}} \left(p^{\frac{k-1}{k}} - p_r^{\frac{k-1}{k}} \right).$$

In virtue of (I.21) and the gas equation (I.12) we may write

$$\varphi_{\text{pol.surf.}} = \frac{k}{1-k} RT + \text{const.} \tag{I.23}$$

The constant value involves the contribution of the lower limit p_r to the integral.

Evaluating the integral for the special case, $k = 1$, that means for the isothermal surface, we get:

$$\varphi_{\text{isoth.surf.}} = - S_o \int_{p_r}^{p} \frac{dp}{p} = - S_o \ln \frac{p}{p_r},$$

but for $k = 1$, (I.21) becomes

$$S_o = RT.$$

Hence

$$\varphi_{\text{isoth.surf.}} = - RT \ln \frac{p}{p_r} \tag{I.24}$$

Finally, the *geostrophic wind equation in polytropic surfaces of class k* ($k \neq 1$) becomes on account of the equations (I.22) and (I.23)

$$\mathbf{v}_g = \mathbf{k} \wedge \frac{1}{\lambda} \underset{\text{pol.surf}}{\nabla} \left(\varphi + \frac{k}{k-1} RT \right) \tag{I.25}$$

φ and T represent the geopotential and temperature distribution for the polytropic surface.

For $k = 1$, the *geostrophic wind equation for isothermal surfaces* is according to (I.22) and (I.24)

$$\mathbf{v}_g = \mathbf{k} \wedge \frac{1}{\lambda} \nabla_T (\varphi + RT \ln p) \tag{I.26}$$

or, in virtue of the gas equation

$$\mathbf{v}_g = \mathbf{k} \wedge \frac{1}{\lambda} \nabla_T (\varphi + RT \ln \rho)$$

T being constant.

By equation (I.25) it is possible to write down the geostrophic wind equations for isentropic and isosteric surfaces immediately.

Substituting for $k = \dfrac{c_p}{c_v}$ in (I.25) it follows that the *geostrophic wind equation in isentropic surfaces* takes the form

$$\mathbf{v}_g = \mathbf{k} \wedge \frac{1}{\lambda} \nabla_\theta (\varphi + c_p T).$$

This equation goes back to Montgomery [1937], who derived it by using the first law of thermodynamics for adiabatic processes:

$$c_p dT - \frac{1}{\rho} dp = 0.$$

The quantity $\psi_M = \varphi + c_p T$ is the isentropic stream function or Montgomery's acceleration potential mentioned earlier, cf. (I.6).

For $k = \infty$, we obtain the *geostrophic wind equation in isosteric surfaces:*

$$\mathbf{v}_g = \mathbf{k} \wedge \frac{1}{\lambda} \nabla_\rho (\varphi + RT) \tag{I.27}$$

or, on account of the gas equation

$$v_g = k \wedge \frac{1}{\lambda} \nabla_\rho \left(\varphi + \frac{p}{\rho}\right)$$

ρ being constant.

It is noteworthy that for $k = 0$ the equation (I.25) reduces to the geostrophic wind equation for isobaric surfaces.

To illustrate the above results a series of aerological charts has been prepared which show the distribution of the stream function for an isobaric, isothermal, isosteric, isentropic and arbitrary surface with geostrophic flow valid for 19 February 1956 15.00 G.M.T.

Chart I represents the 500 mb analysis. Solid lines are contour lines, the broken lines represent isotherms. In the area of interest the temperature distribution indicates a strong baroclinicity of the atmosphere, a condition, which is necessary for getting different stream function distributions. (See section 2).

Chart II shows the distribution of the stream function $\psi = \varphi + RT \ln p$ in an isothermal surface $T = -20°$ C.

Chart III represents the stream function distribution $\psi = \varphi + RT$ for an isosteric surface $\rho = 0.85$ kg m^{-3}.

Chart IV gives the distribution of $\psi = \varphi + c_pT$ for an isentropic surface $\Theta = 24°$ C.

The isopleths for the stream function $\psi =$ const. have been labelled with an increment of 40 gpm. The absolute value of ψ is of no importance, because we may add to it a constant value. The wind data and values for ψ computed from radio sonde and radio-radar wind observations have been inserted in the charts.

According to section 2 the isopleths $\psi =$ const. may be found by the addition of the pattern of surface contour lines and the pattern of surface isobars, after a suitable normalization has been carried through. However, apart from the isosteric surface, the terms which participate in the expression for ψ usually show steep gradients with respect to the gradient in the sum pattern. Consequently in practice the superposition of both patterns meet with some difficulties.

It is evident from the charts that in spite of the strong baroclinicity the structures of the patterns of the stream functions are much alike, except for the isentropic surface.

Finally in chart V a representation is given of the distribution of the stream function for the wind field associated with an arbitrary surface with geostrophic flow. For that purpose the isotherms $-7{,}5°$ C, $-17{,}5°$ C, $-26°$ C, $-35°$ C and $-46{,}5°$ C have been copied from the 850, 700, 600, 500 and 400 mb charts, together with the contour line-elements. These are labelled with an increment of 40 gpm. Afterwards the isopleths for the stream function are drawn free-hand observing the following conditions. The isopleths are tangent to the contour line-elements and the increment of the stream function ψ is equal to the increment of the contour height (40 gpm). Further, the isopleths intersect one and the same isotherm in points of equal contour height. Especially the last two features make a good starting point for the analysis. In chart V the isopleths of the stream function have been drawn free-hand starting from the contour line-elements upon the $-17{,}5°$ C isotherm.

Some wind data which happen to be located at stations at the appropriate positions with respect to the isotherms have been plotted and appear to be in good agreement with the stream function distribution.

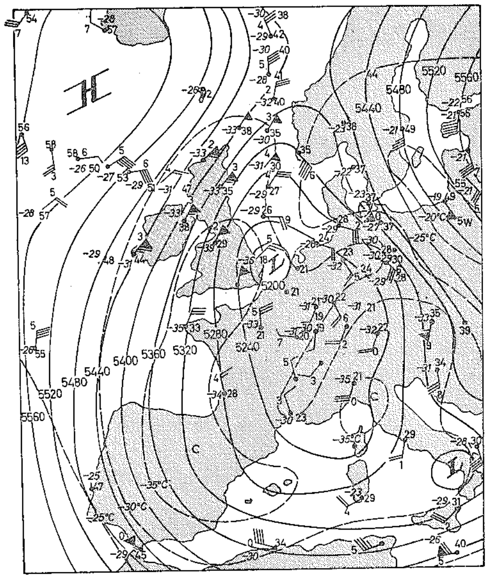

CHART I. 500 mb analysis 19 Febr. 1956, 15.00 G.M.T. Reconnaissance flight, radiosonde and radio radar wind data are plotted in conventional fashion. Geopotential in gp dam, first figure omitted. Solid lines represent contour lines. Increment of geopotential is 40 gpm. Broken lines are isotherms (increment 5° Celsius). L = low, H = high, C = cold, W = warm.

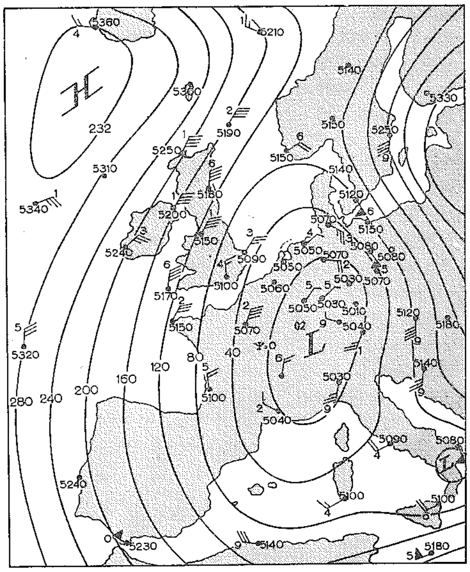

CHART II. Isothermal surface with geostrophic flow for 19 Febr. 1956, 15.00 G.M.T. T = −20° C. Solid lines represent stream lines ψ = const. (increment 40 gpm.) Upper wind data (interpolated from standard levels) are plotted together with computed values of

$$\varphi + RT \ln \frac{p}{p_0}$$

in gpm, where R = 2.8704. 10^6 cm^2 sec^{-2} $°K^{-1}$, p_0 = 1013.2 mb. H = high, L = low.

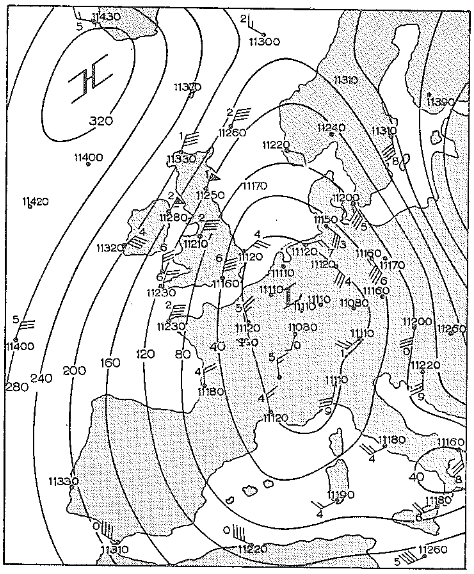

CHART III. Isosteric surface with geostrophic flow for 19 Febr. 1956, 15.00 G.M.T. $\rho = 0.85\,\mathrm{kgm^{-3}}$. Solid lines denote stream lines $\psi = \mathrm{const.}$ (increment 40 gpm). Upper wind data (interpolated from standard levels) as usual. Computed values of $\varphi + RT$ in gpm; $R = 2.8704.10^6$ $\mathrm{cm^2sec^{-2}\ {}^\circ K^{-1}}$. L = low, H = high.

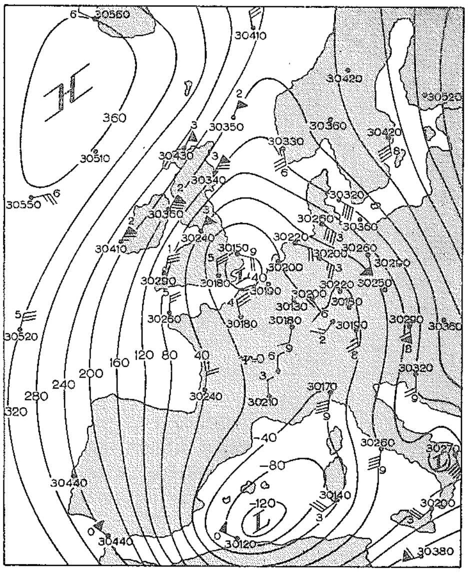

CHART IV. Isentropic surface with geostrophic flow for 19 Febr. 1956, 15.00 G.M.T. $\Theta = 24°$ C. Solid lines represent stream lines $\psi = \mathrm{const.}$ (increment 40 gpm). Upper wind data (interpolated from standard levels) are plotted as well as the computed values of $\varphi + c_pT$ in gpm. $c_p = 10.464.10^6$ $\mathrm{cm^2\ sec^{-2}\ {}^\circ K^{-1}}$. L = low, H = high.

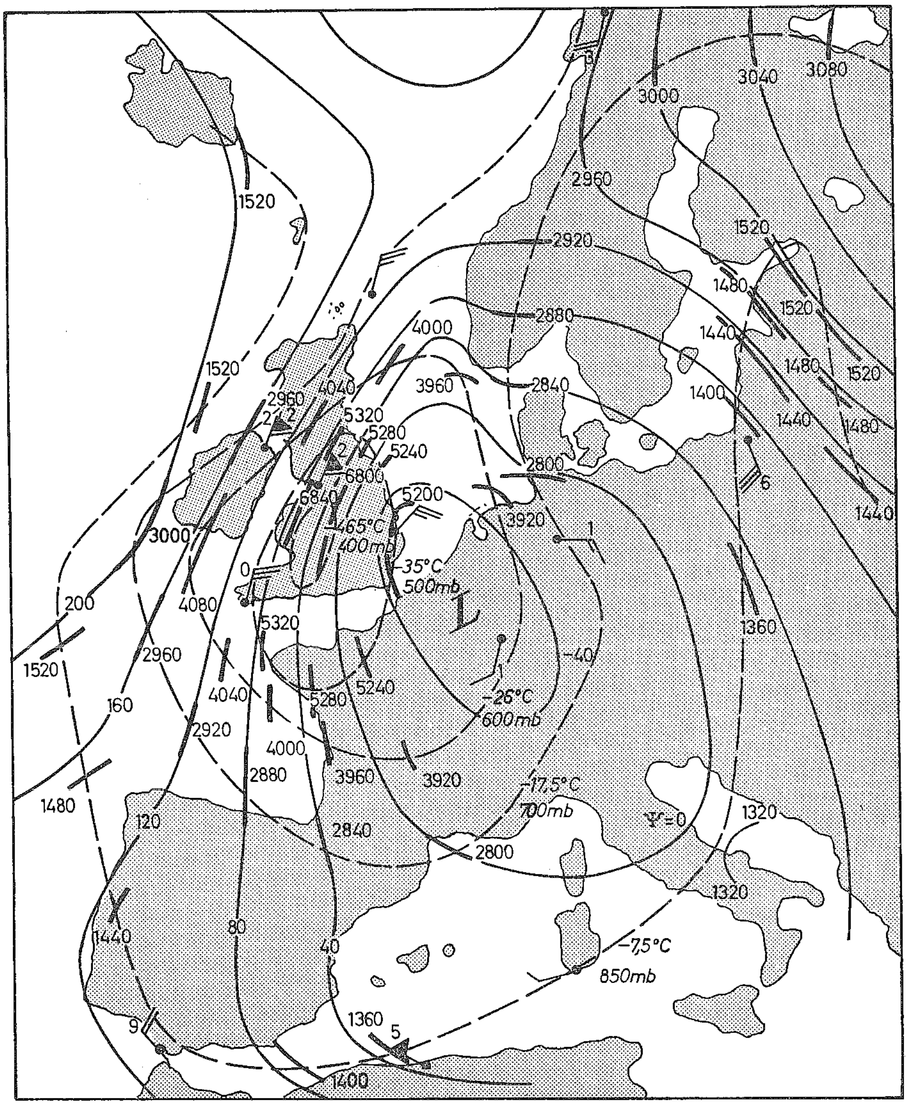

CHART V. Arbitrary surface with geostrophic flow for 19 Febr. 1956, 15.00 G.M.T. Solid lines represent stream lines ψ = const. (increment 40 gpm). Broken lines are isotherms, numbers above line-elements indicate geopotential values on corresponding isobaric surface in gpm. Some wind data are plotted in conventional fashion.

PART II

GEOSTROPHIC FLOW IN NON-STATIONARY AIRFLOW

The upper wind is subject to significant variations in time. Once the geostrophic approximation has been introduced in isobaric or other tolerable surfaces the approximation is justified at any moment.

So, by fixation of one of these surfaces we may investigate under what conditions the velocity field within a composite topography of the surface again possesses a stream function. The problem of composite topographies with geostrophic flow is of importance in aeronautical meteorology, where such a composite topography may be adjusted to the progress of an aircraft's flight.

1. Composite topographies with geostrophic flow

It is an empirical fact that the air flow in the free atmosphere in middle and high latitudes shows a considerable variation in time. As a consequence the accompanying weather phenomena may change rapidly and be spectacular. The flow in isobaric and other physical surfaces is subject to fast alterations in appearance, but it is generally accepted, that the geostrophic approximation is valid every moment. In view of the preceding investigation, which dealt with height-dependent geostrophic flow, it will be obvious to tackle the time-dependent geostrophic flow along the same lines of approach.

Starting with the geostrophic flow in an isobaric surface the geopotential depends not only on the coordinates x and y, but involves in addition a time variable t. Now introduce a "time function" $t = t(x, y)$ and examine whether the flow after substitution for the time function in the field equations may still be conceived as a "geostrophic flow". In other words, try to find a composite topography of the isobaric surface in such a way that the wind distribution is compatible with the concept of geostrophic approximation. Such a procedure gives rise to interesting applications (Parts IV and V).

The geostrophic wind equation on an isobaric surface is determined by the equation

$$\mathbf{v}_g = -\mathbf{k} \wedge \nabla \xi = \mathbf{k} \wedge \frac{1}{\lambda} \nabla_p \varphi,$$

where the stream function $\xi = -\frac{\varphi}{\lambda}$ depends on x, y and t.

After introducing the time function $t = t(x, y)$ we perform a composite windfield $\mathbf{v}_t$:

$$\mathbf{v}_t = -\mathbf{k} \wedge (\nabla \xi)_t,$$

where $(\quad)_t$ means a substitution of the time function $t(x, y)$ in the expression in brackets.

Analogous to expression (I.7) we derive

$$\mathbf{v}_t = -\mathbf{k} \wedge \nabla (\xi)_t + \mathbf{k} \wedge \left(\frac{\partial \xi}{\partial t}\right)_t \nabla t. \tag{II.1}$$

In order that the composite vector field $\mathbf{v}_t$ be derivable from a stream function, the vector field must be non-divergent.

Hence, we investigate

$$\nabla \cdot \mathbf{v}_t = -\nabla \cdot \left(\mathbf{k} \wedge \nabla (\xi)_t\right) + \nabla \cdot \left(\mathbf{k} \wedge \left(\frac{\partial \xi}{\partial t}\right)_t \nabla t\right).$$

According to the vector products:

$$\nabla \cdot \left(\mathbf{k} \wedge \nabla (\xi)_t\right) = \nabla (\xi)_t \cdot \left(\nabla \wedge \mathbf{k}\right) - \mathbf{k} \cdot \left(\nabla \wedge \nabla (\xi)_t\right),$$

$$\nabla \cdot \left(\mathbf{k} \wedge \left(\frac{\partial \xi}{\partial t}\right)_t \nabla t\right) = \left(\frac{\partial \xi}{\partial t}\right)_t \nabla t \cdot \left(\nabla \wedge \mathbf{k}\right) - \mathbf{k} \cdot \left(\nabla \wedge \left(\frac{\partial \xi}{\partial t}\right)_t \nabla t\right)$$

and on account of

$$\nabla \wedge \nabla (\xi)_t \equiv 0$$

and

$$\nabla \wedge \mathbf{k} = 0,$$

we obtain

$$\nabla \cdot \mathbf{v}_t = -\mathbf{k} \cdot \left(\nabla \wedge \left(\frac{\partial \xi}{\partial t}\right)_t \nabla t\right).$$

But, with regard to another vector product, we have

$$\nabla \wedge \left(\frac{\partial \xi}{\partial t}\right)_t \nabla t = - \nabla t \wedge \nabla \left(\frac{\partial \xi}{\partial t}\right)_t.$$

Hence,

$$\nabla \cdot \mathbf{v}_t = \mathbf{k} \cdot \nabla t \wedge \nabla \left(\frac{\partial \xi}{\partial t}\right)_t.$$

The term on the right is a triple scalar product, that may be expressed in the form

$$\nabla \cdot \mathbf{v}_t = J \left(t, \frac{\partial \xi}{\partial t}\right),$$

where J represents the Jacobian determinant in the horizontal plane

$$J \left(t, \frac{\partial \xi}{\partial t}\right) = \frac{\partial}{\partial (x, y)} \left(t, \frac{\partial \xi}{\partial t}\right).$$

Replacing ξ by $-\dfrac{\varphi}{\lambda}$ condition $\nabla \cdot \mathbf{v}_t = 0$ in isobaric surfaces may be written

$$J \left(t, \frac{\partial \varphi}{\partial t}\right) = 0, \tag{II.2}$$

which is the abbreviated form of the partial differential equation

$$\varphi_{ty} \frac{\partial t}{\partial x} - \varphi_{tx} \frac{\partial t}{\partial y} = 0 \tag{II.3}$$

It turns out that the time function $t = t(x, y)$ should be a solution of this equation.

The condition (II.2) means geometrically, that the isochronals $t =$ constant should coincide with the issallopleths $\dfrac{\partial \varphi}{\partial t} =$ const. (issallo-geopotential lines) at the moment t.

Since the coëfficients φ_{tx} and φ_{ty} involve the variable t the equation (II.3) is a homogeneous quasi-linear partial differential equation. The general solution consists of a relationship $\pi = 0$ between t and $\dfrac{\partial \varphi}{\partial t}$

$$\pi\left(t, \frac{\partial\varphi}{\partial t}\right) = 0.$$

Rather for convenience this relationship may be written in the form

$$\frac{\partial\varphi}{\partial t} = -\frac{d\varphi^*}{dt}, \tag{II.4}$$

where $\varphi^* = \varphi^*(t)$ is an arbitrary (differentiable) function of t only.

The geostrophic equation for the windfield in the composite topography is then in terms of (II.1)

$$\mathbf{v}_g = \mathbf{v}_t = \mathbf{k} \wedge \frac{1}{\lambda} \nabla_t \varphi + \mathbf{k} \wedge \frac{1}{\lambda}\left(\frac{d\varphi^*}{dt}\right)_t \nabla t$$

$$= \mathbf{k} \wedge \frac{1}{\lambda} \nabla_t \varphi + \mathbf{k} \wedge \frac{1}{\lambda} \nabla_t \int_{t_o}^{t} \frac{d\varphi^*}{dt} dt,$$

where t_o denotes any fixed initial instant.

Hence, we have

$$\mathbf{v}_g = \mathbf{k} \wedge \frac{1}{\lambda} \nabla_t (\varphi + \varphi^*). \tag{II.5}$$

The windfield in the composite topography therefore possesses a stream function

$$\chi = (\varphi + \varphi^*)_t. \tag{II.6}$$

We may summarize our results as follows:

In an isobaric surface with geostrophic flow the windfield in a composite topography of the isobaric surface, defined by the time function $t = t(x, y)$, behaves like geostrophic flow, if the time function is a solution of the partial differential equation

$$J\left(t, \frac{\partial\varphi}{\partial t}\right) = 0.$$

The geostrophic wind equation takes the form

$$\mathbf{v}_g = \mathbf{k} \wedge \frac{1}{\lambda} \nabla_t \chi,$$

where χ represents the sum of the geopotential φ of the composite topography of the isobaric surface and φ^* which denotes some arbitrary function of t. The time function is determined by the relation

$$\frac{\partial \varphi}{\partial t} = - \frac{d\varphi^*}{dt}.$$

The isochrones t = constant coincide with issallo-contourlines (issallohypses) $\dfrac{\partial \varphi}{\partial t}$ = const. at the moment t.

For a graphical representation of the composite topography with geostrophic flow two sets of lines would suffice, namely the set of composite contours $(\varphi)_t$ = constant and the set of isochronals t = constant, provided that the isochronals are labelled according to time and tendency (fig. 2). The location

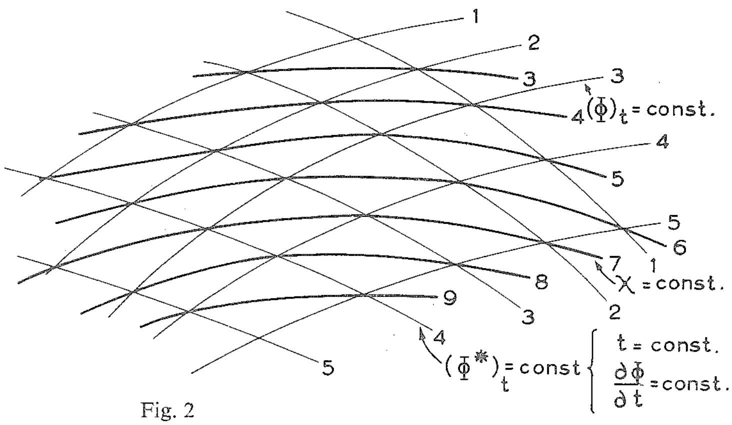

Fig. 2

of the wind may be read from the topography contours and isochronals. The wind itself may be found by computation according to equation (II.5). To avoid this computation a third set of lines may be added, consisting of the stream lines $(\varphi + \varphi^*)_t$ = constant. This set may be found by carrying out a graphical addition in the patterns of composite contours and isochronals, after $(\varphi)_t$ and $(\varphi^*)_t$ have been normalized properly, that means after $(\varphi)_t$ and $(\varphi^*)_t$ are expressed in the same unit and the increment of $(\varphi)_t$ is equal to the increment of $(\varphi^*)_t$ (fig. 2).

2. Differential analysis

With respect to isobaric surfaces there is a principle type of differential analysis from one surface to another, that is very useful because of its relation to hydrostatics. The differential analysis of the topographies of two different isobaric surfaces for the same time gives the pattern of thickness for the layer. The differential lines obtained by subtracting the two patterns are *relative contours* or *thickness lines.*

From the hydrostatic equation (I.11) and the gas equation (I.12) it follows, that the geopotential difference $\triangle \varphi$ between two isobaric surfaces $p_1 = \text{const.}$ and $p_2 = \text{const.}$ becomes

$$\triangle \varphi = - R\overline{T}_v \ln \frac{p_1}{p_2}, \qquad \text{(II.7)}$$

where $\overline{T}_v$ denotes the mean virtual temperature for the layer. The relative contour lines may therefore be interpreted as *mean virtual isotherms.* The gradient pattern associated with the field of mean virtual isotherms determines the geostrophic approximation of the *thermal wind* pattern.

The above differential analysis for isobaric surfaces is commonly used in meteorological practice. Most often the topography of a *standard* isobaric surface, e.g. the 500 mb surface, is derived from the topography of a lower *standard* isobaric surface, e.g. 1000 mb surface, by adding graphically the thickness pattern between the two standard levels, i.e. the layer between 1000 and 500 mb.

In view of the concept of composite topographies with associated geostrophic flow we may put the question whether the method of differential analysis still holds in composite topographies.

Supposing that φ_1 represents the geopotential in the lower pressure surface $p_1 = \text{constant}$, φ_2 the geopotential in the upper pressure surface $p_2 = \text{constant}$ and φ the geopotential difference or thickness for the layer between the pressure levels p_1 and p_2.

Then we have constantly

$$\varphi_2 = \varphi_1 + \varphi. \qquad \text{(II.8)}$$

We perform a composite topography of the lower pressure level by introducing a time function $t = t(x, y)$. The associated windfield behaves like geostrophic flow, if the time function is a solution of the partial differential equation

$$J\left(t, \frac{\partial\varphi_1}{\partial t}\right) = 0.$$

According to (II.4) the time function is determined by the equation

$$\frac{\partial\varphi_1}{\partial t} = -\frac{d\varphi_1^*}{dt} \tag{II.9}$$

where φ_1^* is an arbitrary function of t.

At the same time we prepare a composite thickness topography with geostrophic flow. Then it follows from (II.4) that the time function should also be a solution of the equation

$$\frac{\partial\varphi}{\partial t} = -\frac{d\varphi^*}{dt} \tag{II.10}$$

where φ^* denotes another arbitrary function of t.

Owing to the fact, that both φ^* and φ_1^* represent functions of t only, the time functions can be solutions of (II.9) and (II.10) simultaneously, provided that

$$\frac{\partial\varphi}{\partial t} = g(t)\,\frac{\partial\varphi_1}{\partial t},\ g \text{ arbitrary.}$$

As a result we observe that the graphical addition according to the method of differential analysis preserves its validity for composite topographies with geostrophic flow, if the tendency pattern of the geopotential of the lower pressure surface and the tendency pattern of the mean virtual temperature for the layer be *similar* or *homomorph* at any moment. On account of (II.8) both patterns will also be homomorph with the tendency pattern of the geopotential of the upper pressure surface.

In virtue of (II.8) we have

$$J\left(t, \frac{\partial\varphi_2}{\partial t}\right) = J\left(t, \frac{\partial\varphi_1}{\partial t} + \frac{\partial\varphi}{\partial t}\right) = J\left(t, \frac{\partial\varphi_1}{\partial t}\right) + J\left(t, \frac{\partial\varphi}{\partial t}\right) = 0,$$

showing that in case of homomorphy of the tendency patterns the time function satisfies the partial differential equation for geostrophic flow in the composite topography of the upper pressure surface.

In autobarotropic atmospheres, where the wind distribution in a pressure surface is independent of the pressure variable, the condition of homomorphy is automatically fulfilled. In the real atmosphere, however, the tendency patterns may be far from being homomorph. Examination of charts which represent height changes of pressure surfaces and changes of thickness for the associated isobaric layer, indicate that the broad scale features like areas of lowering geopotential and decreasing thickness are more or less coincident, but minor features of the pattern may differ considerably. For instance, the location of the points of maxima and minima seem often to divert from the vertical.

3. The enveloping topography of isobaric surfaces

Returning to the simple homogeneous quasi-linear partial differential equation (II.3) we note that this equation yields a particular solution for the time function, which enables us to study the enveloping topography of a pressure surface.

By taking $\varphi^* = 0$ in (II.4) the time function t(x, y) is determined by the equation

$$\frac{\partial \varphi}{\partial t} = 0. \qquad \text{(II.11)}$$

Differentiation with respect to x and y gives

$$\varphi_{tx} + \varphi_{tt} \frac{\partial t}{\partial x} = 0,$$

$$\varphi_{ty} + \varphi_{tt} \frac{\partial t}{\partial y} = 0.$$

Elimination of φ_{tt} from these equations shows that the time function satisfies the partial differential equation (II.3). Hence this special time function defines a particular composite topography, c.q. *enveloping topography*, which involves the following properties (fig. 3).

1) The isochronals coincide with the zero issallo geopotential lines or zero issallohypses.
2) The stream lines are enveloping curves of the contour lines.
3) The geostrophic wind is determined by the composite stream function $\varphi(x, y, t(x, y))$.

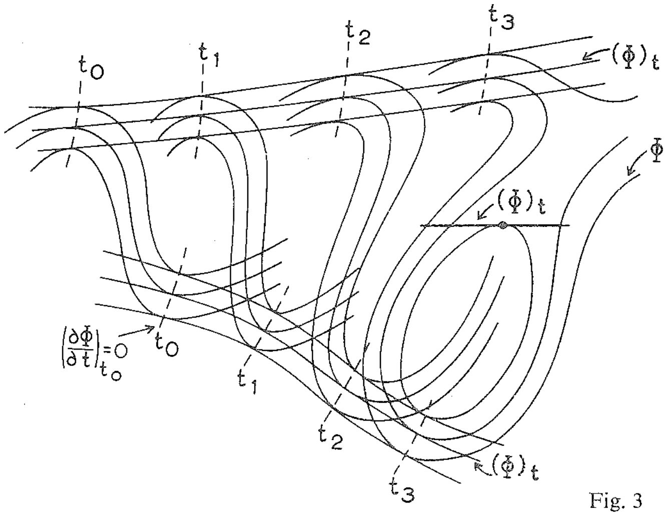

Fig. 3

The first property is inferred from (II.2), the second from the remark, that the stream lines are found by elimination of t from $\frac{\partial \varphi}{\partial t} = 0$ and $\varphi(x,y,t) =$ const., the third from the geostrophic wind equation (II.5) which, in virtue of $\varphi^* = 0$ takes the form

$$\mathbf{v}_g = \mathbf{k} \wedge \frac{1}{\lambda} \nabla_t \varphi$$

To demonstrate the theory we will investigate the enveloping topographies associated with the severe gale which caused the disastrous floods along the North Sea coasts of England, Belgium and Holland Jan. 31–Febr. 1 1953. A full account of the meteorological situation has been described elsewhere, van der Ham [1953].

Chart VI represents the enveloping topography of the 1000 mb chart or surface weather chart. It involves the enveloping isobars with an increment of 5 mb ($\sim$ 40 gpm). Apart from that the zero-issallobars have been drawn and some pressure and wind data inserted which correspond to the time along the issallobars. The track of the centre of the depression is the curve which connects the angular points of the enveloping isobars. Deepening of the depression is reflected in the figure by a divergence of the isobars and the lack of the position of zero-issallobars behind the depression centre. Filling of the depression is reflected by a convergence of isobars and the lack of the depression centre behind the position of the zero-issallobars. Near Scotland a secondary depression centre develops, but this centre has a short lifetime and is taken up by a deep trough moving to North Germany. Near the Dutch coast a crowding of the isobars appears, which is associated with the trough at the time that the winds reach gale force along the Dutch coast.

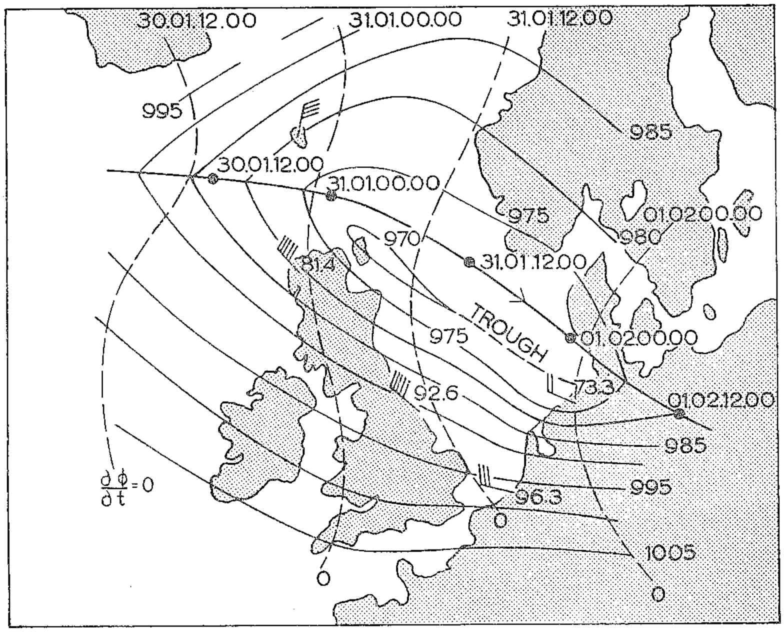

CHART VI. Enveloping topography of the surface weather chart for 30 Jan. 1953, 12.00 G.M.T. – 1 Febr. 1953, 12.00 G.M.T. Solid lines represent enveloping isobars (increment 5 mb.) Broken lines represent isochrones – zero issallobars. Numbers near location of centres and isochrones give date and time. Wind data and pressure values as usual.

Chart VII represents the enveloping topography of the 700 mb pressure level. The enveloping contour lines are labelled with an increment of 40 gpm. The broken lines represent zero-issallohypses, which connect the tangent points of contours and enveloping contours. Along these zero-issallohypses the appropriate time data have been inserted in the chart. Apart from that chart VII contains composite isotherms. The hatched area indicates a tongue of cold air.

Finally chart VIII illustrates the enveloping topography of the 500 mb pressure level with the same elements as in chart VII.

Comparing the three charts they present some interesting features. The track of the centre of the depression at 700 and 500 mb as well as the track of the secondary centre on the surface map are practically coincident. The track of the main centre of the surface depression is displaced to the north. The tracks almost run parallel to the enveloping contours. The instants, at which the minimum pressure value is reached in the centre, show a retardation towards higher levels. Moreover, the centres of minimum pressure are displaced down stream at higher levels. In other words, the depression pierces through the atmosphere from lower to higher levels. Examination of the composite temperature distribution shows that an influx of cold maritime polar air occurs south of the centre. At the same time relative warm

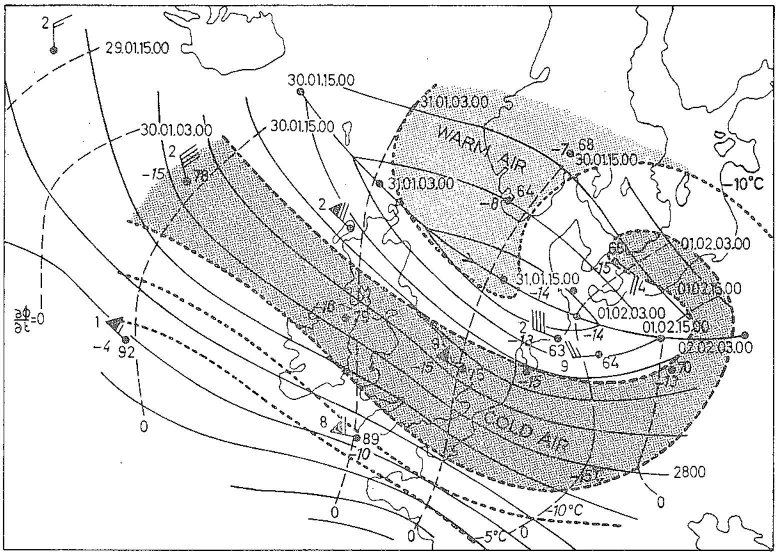

CHART VII. Enveloping topography of 700 mb pressure surface for 29 Jan. 1953, 15.00 G.M.T. – 2 Febr. 1953, 03.00 G.M.T. Solid lines represent enveloping contours (increment 40 gpm). Broken lines are isochrones – zero issallohypses. Dotted lines represent composite isotherms (increment 5° C). Some upper air data are plotted as before. Hatched area denotes a tongue of cold air. Dotted portion denote a tongue of relatively warm air.

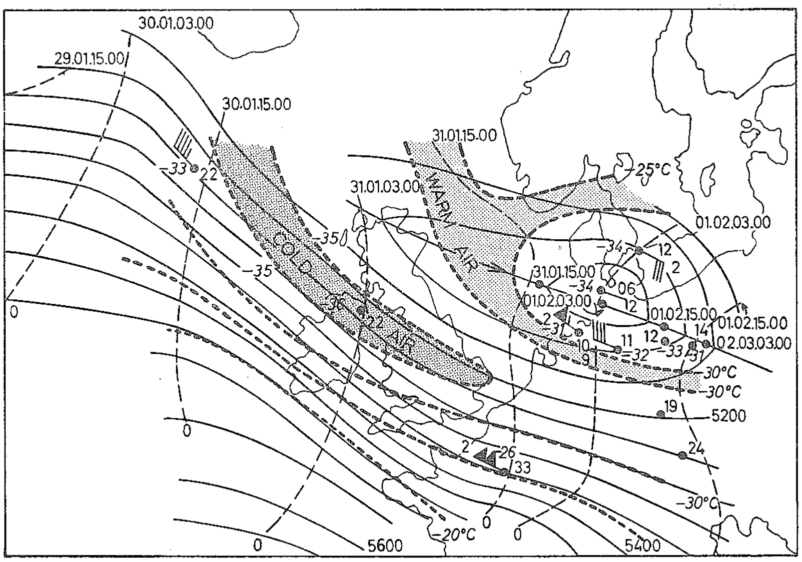

CHART VIII. Enveloping topography of 500 mb pressure surface for 29 Jan. 1953, 15.00 G.M.T. – 2 Febr. 1953, 03.00 G.M.T. Solid lines are enveloping contours (increment 40 gpm.) Broken lines represent isochrones – zero issallohypses. Dotted lines are composite isotherms (increment 5° C). Hatched area represents tongue of cold air. Upper air data plotted in conventional fashion. Dotted portion indicates tongue of relatively warm air.

air floats in from a location north of the centre in between the centre and tongue of cold air, a situation which often gives rise to severe gales, Bijvoet [1956].

The above example shows that by means of enveloping topographies a number of special features of the meteorological situation can be compiled in complete form.

PART III

GEOSTROPHIC APPROXIMATION IN GENERAL

When the geostrophic flow is considered to be valid with respect to time and pressure the problem dealt with in the two previous parts may be extended by studying composite velocity fields in space and time, which again may be described by a stream function.

1. Space-time geostrophic approximations

In the previous section we investigated composed topographies of isobaric surfaces with geostrophic flow. The theory was based on the empirical fact that the geostrophic approximation in isobaric surfaces is independent of time. The restriction to isobaric surfaces seems to be rather fortuitous because we have shown that the geostrophic approximation also holds for other physical surfaces, like isothermal, isosteric and isentropic surfaces, in general for all scalar surfaces S = constant, which are generated by coinciding isobaric, isothermal and isosteric lines. (Part I, section 2).

Apparently we may extend the theory in terms of composite topographies of these scalar surfaces. In so doing it suffices to replace the geopotential φ in (II.2) and (II.5) by the stream function $\psi = \varphi - \varphi_{S_0}$. As a result we have: In scalar surfaces S = const. with geostrophic flow

$$\mathbf{v}_g = \mathbf{k} \wedge \frac{1}{\lambda} \nabla_{s,t} \psi$$

the wind pattern in a composite topography of these surfaces defined by the time function t = t(x, y), behaves like geostrophic flow if the time function is a solution of the partial differential equation

$$J\left(t, \frac{\partial \psi}{\partial t}\right) = 0.$$

The geostrophic equation takes the form

$$\mathbf{v}_g = \mathbf{k} \wedge \frac{1}{\lambda} \nabla_t (\psi + \psi^*),$$

where ψ represents the stream function for the geostrophic flow in the scalar surface and ψ^* denotes an arbitrary function of time. The associated time function is determined by the relation

$$\frac{\partial \psi}{\partial t} = - \frac{d\psi^*}{dt}$$

We observe that the above extension of the theory only involves a special aspect of the problem to investigate space-time geostrophic approximations and that, apart from the composite topographies of the specified scalar surfaces with geostrophic flow, other wind configurations exist which behave like geostrophic flow.

To explain this we return to the geostrophic wind equation

$$\mathbf{v}_g = - \mathbf{k} \wedge \nabla \xi = \mathbf{k} \wedge \frac{1}{\lambda} \nabla_{p,t} \varphi.$$

The suffixes p and t now indicate that the geostrophic equation is justified at any moment and on every isobaric surface.

We create a composite wind configuration by introducing a time function $t = t(x, y)$ and space function $p = p(x, y)$.

The windvector in the composite configuration becomes:

$$\mathbf{v} = - \mathbf{k} \wedge (\nabla \xi)_{p,t} = - \mathbf{k} \wedge \nabla(\xi)_{p,t} + \mathbf{k} \wedge \left(\frac{\partial \xi}{\partial p}\right)_{p,t} \nabla p + \mathbf{k} \wedge \left(\frac{\partial \xi}{\partial t}\right)_{p,t} \nabla t,$$

where $(\quad)_{p,t}$ denotes, as before, a substitution of the time- and space function in the expression in brackets.

The resulting wind pattern behaves like geostrophic flow, if the vector configuration is non-divergent. Thus we have the condition:

$$\nabla \cdot \mathbf{v} = - \nabla \cdot \left(\mathbf{k} \wedge \nabla (\xi)_{p,t}\right) + \nabla \cdot \left(\mathbf{k} \wedge \left(\frac{\partial \xi}{\partial p}\right)_{p,t} \nabla p\right) + \nabla \cdot \left(\mathbf{k} \wedge \left(\frac{\partial \xi}{\partial t}\right)_{p,t} \nabla t\right) = 0$$

On account of

$$\nabla \cdot \left(\mathbf{k} \wedge \nabla (\xi)_{p,t}\right) = \mathbf{k} \cdot \left(\nabla \wedge \nabla (\xi)_{p,t}\right) \equiv 0$$

we have

$$\left(\frac{\partial\xi}{\partial p}\right)_{p,t} \nabla p \cdot (\nabla \wedge \mathbf{k}) - \mathbf{k} \cdot \left(\nabla \wedge \left(\frac{\partial\xi}{\partial p}\right)_{p,t} \nabla p\right) +$$

$$\left(\frac{\partial\xi}{\partial t}\right)_{p,t} \nabla t \cdot (\nabla \wedge \mathbf{k}) - \mathbf{k} \cdot \left(\nabla \wedge \left(\frac{\partial\xi}{\partial t}\right)_{p,t} \nabla t\right) = 0.$$

But according to

$$\nabla \wedge \mathbf{k} = 0$$

this equation reduces to the form:

$$\mathbf{k} \cdot \nabla p \wedge \nabla \left(\frac{\partial\xi}{\partial p}\right)_{p,t} + \mathbf{k} \cdot \nabla t \wedge \nabla \left(\frac{\partial\xi}{\partial t}\right)_{p,t} = 0 \qquad \text{(III.1)}$$

which expresses that the time function t(x, y) and space function p(x, y) must satisfy the partial differential equation

$$\xi_{px} \frac{\partial p}{\partial x} - \xi_{py} \frac{\partial p}{\partial y} + \xi_{tx} \frac{\partial t}{\partial y} - \xi_{ty} \frac{\partial t}{\partial x} = 0.$$

Using the Jacobi-determinant terminology, (III.1) may be written

$$J\left(p, \frac{\partial\xi}{\partial p}\right) + J\left(t, \frac{\partial\xi}{\partial t}\right) = 0$$

and in view of

$$\xi = -\frac{\varphi}{\lambda}$$

we finally have

$$J\left(p, \frac{\partial\varphi}{\partial p}\right) + J\left(t, \frac{\partial\varphi}{\partial t}\right) = 0. \qquad \text{(III.2)}$$

The result may be summarized as follows:
A composite wind configuration in space and time defined by the time function t(x,y) and space function p(x,y) is a geostrophic wind configuration, if the time and space function are solutions of the partial differential equation (III.2).

It is evident that for $t \equiv$ constant we have to deal with surfaces with geostrophic flow, for which

$$J\left(p, \frac{\partial \varphi}{\partial p}\right) = 0$$

and for $p \equiv$ const. we have the special case of composite topographies of isobaric surfaces with geostrophic flow, for which

$$J\left(t, \frac{\partial \varphi}{\partial t}\right) = 0.$$

The partial differential equation (III.2)
rewritten for φ:

$$\varphi_{px} \frac{\partial p}{\partial y} - \varphi_{py} \frac{\partial p}{\partial x} + \varphi_{tx} \frac{\partial t}{\partial y} - \varphi_{ty} \frac{\partial t}{\partial x} = 0 \qquad \text{(III.3)}$$

is a rather peculiar one, inasmuch it involves two independent variables p and t. We will not attempt to find a general solution, but restrict ourselves to the examination of a particular one.

Let an arbitrary isobaric surface $p = p_o$ be given. A composite topography of this surface with geostrophic flow is formed by introducing a time function $t = t(x,y; p_o)$, which is

a solution of equation (II.2)

$$J_{p_o}\left(t, \frac{\partial \varphi}{\partial t}\right) = 0,$$

where the suffix p_o indicates that J refers to the isobaric surface $p = p_o$. The time function will be determined by the relation (II.4)

$$\frac{\partial \varphi}{\partial t} = - \frac{\partial \varphi^*}{\partial t},$$

where φ^*, besides containing the "parameter" p_o, is an arbitrary function of t, $\varphi^* = \varphi^*(p, t)$. The stream function associated with the specified composite topography is according to (II.6)

$$\chi = (\varphi + \varphi^*)_t.$$

If p_o is made to vary, we have a set of composite topographies of isobaric surfaces with geostrophic flow, appropriate time functions $t = t(x,y; p)$ and associated stream functions $\chi = \chi(x,y; p)$. In the set of composite topographies we now try to perform a new geostrophic approximation by selecting a space function $p = p(x, y)$ in such a way that $p = p(x, y)$ and the time function $t = t(x, y, p(x, y))$ solve the equation (III.3).

Without going into detail it is proved that $p(x, y)$ must be a solution of the equation

$$J\left(p, \frac{\partial \chi}{\partial p}\right) = 0.$$

The space function of the resulting geostrophic wind configuration is then determined by the relation

$$\frac{\partial \chi}{\partial p} = -\frac{d\chi^*}{dp}, \chi^* = \chi^*(p),$$

while the associated stream function $\mathfrak{z}$ becomes

$$\mathfrak{z} = (\chi + \chi^*)_p$$

or

$$\mathfrak{z} = (\varphi + \varphi^*)_{p,t} + (\chi^*)_p. \tag{III.5}$$

This fairly complicated particular solution will be applied in part IV.

By reason of symmetry another particular solution may be found, by simply interchanging the variables p and t in the above demonstration.

It can be shown, that, in virtue of the last argument, the partial differential equation (III.3) involves among other solutions the composite topographies of scalar surfaces with geostrophic flow, as should be the case.

PART IV

APPLICATION IN AERONAVIGATION

In aeronautical meteorology different objectives in altimetry and pressure pattern technique are attached to the concept of geostrophic winds and geostrophic flow. Amongst them may be mentioned the determination of drift from altimeter observations, the evaluation of wind components along fixed routes, the use of D-value, the pre-flight planning of long distance flights and single heading flight navigation or constant drift course. There still remain a number of problems to be solved and in addition some new problems arise due to the fact that operations with piston engined aircraft are gradually replaced by those of turbo prop and turbo jet powered aircraft. In this part some of these problems will be studied taking into account the results obtained in the previous parts concerning geostrophic flow.

1. Composite charts

In practice the flight-planning of long distance flights with piston-engined aircraft is generally performed by means of *fixed time* pressure contour analysis and *prontours* of selected standard pressure surfaces, for instance the 700, and 500 mb charts. As the total flight time of these aircraft often amounts to more than 10 hours, important factors for the flight planning like wind and temperature distribution are subject to considerable changes in time during the progress of the flight. As a consequence the fixed time charts give an erroneous picture of the situation along the track. In order to avoid this difficulty, *composite* pressure contour charts and prontours have been introduced which involve a representation of temperature and wind in such a way that the situation at an arbitrary point of the track is nearby the expected situation at the time that the aircraft will be at that point.

With regard to long distance flights with turbo prop and turbo jet-powered aircraft the total flight time is reduced to half the corresponding flight time for piston engined aircraft. Consequently the variation in time of wind and temperature distribution will have a less serious effect on the preparation of the flight.

However, a particular characteristic should be taken into account. As the most economic flight procedure is obtained by performing a continuous cruise climb or stepped climb, the flights take place on sloping surfaces which deviate considerably from an isobaric surface. Therefore it is obvious to introduce *composite charts in space*. Since the notion of composite charts up to the present lacks clarity, it will be the aim of this part to relate the concept of composite charts to that of the geostrophic flow dealt with in the previous parts.

2. Composite charts in time

In order to apply the concept of geostrophic flow for aeronautical purposes it is essential to relate the navigational aspects to the representation of meteorological elements which control the progress of the flight.

Assuming flights in isobaric surfaces, i.e. flights at a constant pressure altitude, we may investigate the relationship by means of some simple geometrical considerations.

Without any specification of the navigation system there is no possibility to introduce composite charts. This may be shown by examination of fig. 4.

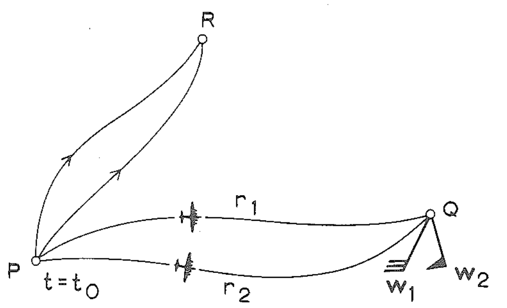

Fig. 4

Let an aircraft, starting from P at time $t = t_o$, be navigated along track r_1, to a point Q. The aircraft will arrive at Q at time $t = t_1$. At time t_1 the windvector in Q be w_1. The same aircraft could have been directed along another track r_2 by using another navigation method. Then the time of arrival would be $t = t_2$. On account of the time variability of the wind the windvector in Q at $t = t_2$ will be w_2. The windvector in Q thus depends on the navigation system. The same holds good for other points R in the area of interest, showing that it is impossible to have a composite chart which accounts for the distribution of wind and other elements for different navigation systems simultaneously.

If, however, a particular navigation system is considered a composite chart is capable of representing the situation along the track.

To explain this, we recall that the pressure pattern tracks associated with a specified navigation system may be arranged in *complete figures*. These figures consist of a one-parameter family of tracks and associated pattern of timefronts. (fig. 5). The timefronts are unfolding and originate from an arbitrary curve or

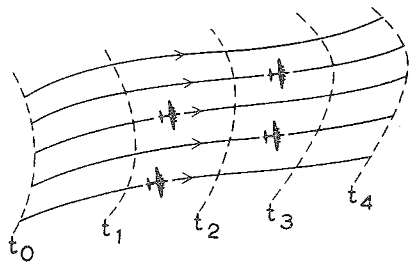

Fig. 5

point (fig. 6), de Jong [1956]. A special method for the construction of the

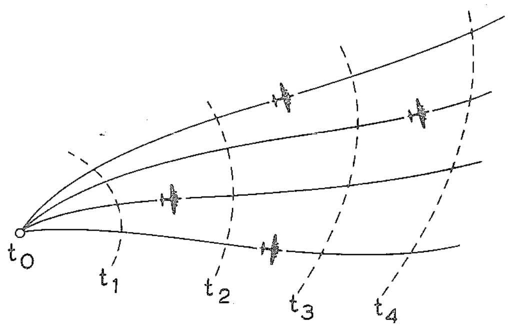

Fig. 6

pressure pattern tracks, minimum flight paths for instance, is actually based on the principle of propagation of timefronts.

Comparing the complete figures with composite topographies it is obvious to introduce a composite chart for a complete figure by identifying the timefronts with isochronals of the composite chart. Such a composite topography will not have geostrophic flow, because the isochronals in general will not coincide with issallohypses. In such a composite chart the windfield is therefore not derivable from a streamfunction. Consequently it can only be described by means of isotachs, stream lines, convergence-, divergence- and neutral points etc., similar to the representation of the wind distribution in tropical regions.

Further, we may consider a specified pressure pattern track between two points P and Q (fig. 7). The flight proceeds in time according to t = t(s), where s

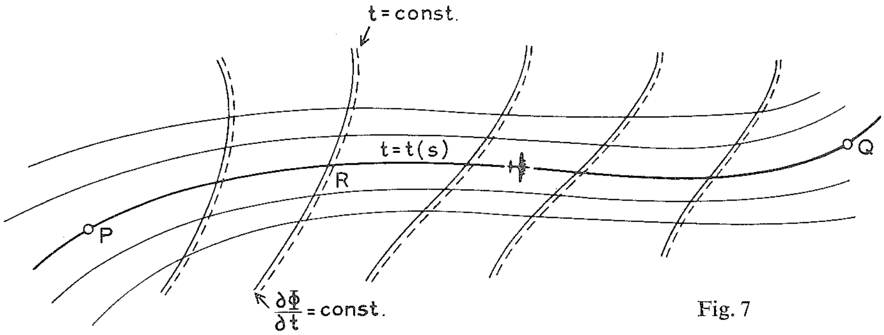

Fig. 7

denotes a suitable parameter, for instance the arc distance. Through any point R we may draw an isochrone for which t = t(s(R)) = constant. If R is made to run over the track a time function t is found which on the track takes the value t = t(s). This time function defines a composite topography within which the track is embedded. The composite chart is not uniquely determined because the selection of isochrones is arbitrary. As a special case however we may take the isochrones which coincide with issallohypses. Then a composite chart with geostrophic flow results. Any pressure pattern track associated with a specified navigation system may therefore be embedded in a composite chart with geostrophic flow. Summarizing our results we observe that *in aeronavigation composite isobaric charts may be introduced only for complete figures associated with a specified navigation system. Apart from that each specified flight in an isobaric surface may be embedded in a composite topography with geostrophic flow.*

It is noteworthy that this result is also valid for flights within other physical surfaces with geostrophic flow, for instance within polytropic surfaces and in general within scalar surfaces, which are generated by coinciding isobars, isotherms and isosteric lines.

3. Composite charts in space

Especially in view of turbo prop and turbo jet-powered aircraft the problem arises, whether suitable composite charts in space may be introduced for the purpose of flight analysis and pre-flight planning.

In the first instance we tackle this problem by considering fixed time charts and restrict ourselves to the examination of a specific flight associated with a particular system of navigation. Let us suppose that the track between the points P and Q be r. (fig. 8). Through any point R of this track we may draw

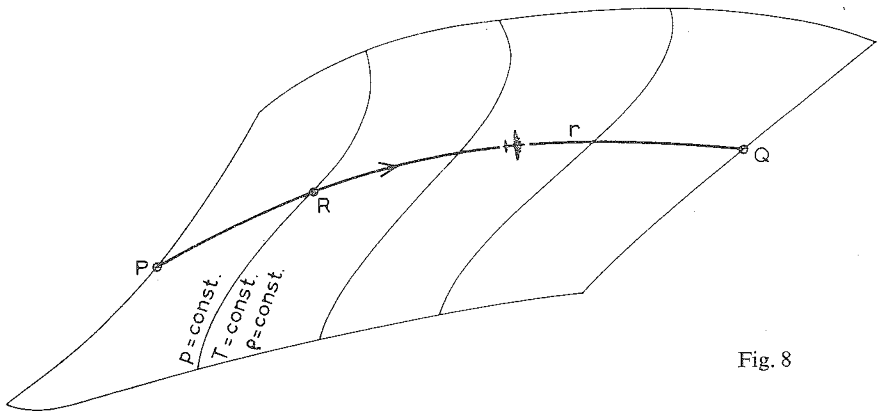

Fig. 8

coinciding isobars, isotherms and isosteric lines, along which $p = \text{const.}$, $T = \text{const.}$ and $\rho = \text{const.}$ As these lines happen to be the characteristic curves of surfaces with geostrophic flow (Part I, section 2) these lines generate a uniquely defined surface (Cauchy's problem). Thus we have

In a stationary or quasi-stationary airflow any pressure pattern track may be embedded in a surface with geostrophic flow.

4. Composite charts in space and time

When the upper air flow is subject to considerable variations in time with respect to the overall flight duration we may put the question whether an arbitrary pressure pattern track may still be embedded in a geostrophic wind configuration. The answer is in the affirmative.

To demonstrate this we refer to Part III. Let r again be a pressure pattern track between P and Q. Upon this track a pressure distribution $p = p(s)$ and progress of time $t = t(s)$ appear. Now we consider an arbitrary point R. Point R is located at a pressure surface $p = p(s(R)) = \text{const.}$ In this pressure surface we create a composite topography with geostrophic flow by introducing a time function t(x, y, p(s(R))), which is a solution of the partial differential equation

$$J_p\left(t, \frac{\partial\varphi}{\partial t}\right) = 0.$$

The solution is specified in such a manner that the isochronal passing through R, indicates the time $t = t(s(R))$. This may be accomplished by the choice of the function $\varphi^*(t)$. The associated stream function is $\chi = (\varphi + \varphi^*)_t$. If the point R is made to run along the pressure pattern track a set of composite topographies of isobaric surfaces with geostrophic flow is found, with appropriate time functions $t = t(x, y, p(s))$ and associated stream functions

$$\chi = \chi\big(x, y, p(s)\big) = \big(\varphi + \varphi^*\big)_t.$$

In this set of composite topographies we then perform a new geostrophic approximation by taking a space function $p = p(x, y)$ which is a solution of the equation

$$J\left(p, \frac{\partial\chi}{\partial p}\right) = 0$$

and specify the space function in such a way that the (composite) isobar, passing through a point R, indicates the pressure $p = p(s(R))$. Again this may be accomplished by specifying function χ^* in the right manner. The resulting composite wind configuration is a geostrophic wind configuration because the above description fully agrees with the construction of a particular solution of the differential equation (III.3) for geostrophic wind configurations in time and space.

Hence we may state
any pressure pattern track may be embedded in a geostrophic wind configuration.

5. Composite charts in practice

It has been shown that every pressure pattern track may be embedded in geostrophic motion. Thus, great circle track, single heading track, rhumbline track and minimum flight path may in principle be analysed within composite charts with geostrophic flow. But obviously the conditions which such composite charts have to satisfy are difficult to realise in practice. Besides, the prognostic character of pre-flight planning implies the necessity to consider prognostic upper air charts or *prontours*, the preparation of which should be based on dynamical and physical reasoning. For this purpose a number of statistical, numerical and graphical methods has been designed (cf. Reuter [1954]). Especially the development of numerical forecasts in model atmospheres by means of electronic computers has made considerable progress.

Speaking of composite charts in practice one usually is understood to mean by that a composite topography of an isobaric surface

$$\varphi = \varphi\big(x, y, t(x, y)\big)$$

where t(x, y) has been adjusted to the progress of flight, most likely in the given situation. As has been demonstrated in part II the geostrophic wind, derived from this composite topography, involves only a part of the actual wind, i.e. the part that refers to the first term in the right side of the wind equation (II.1)

$$\mathbf{v}_g = \mathbf{k} \wedge \frac{1}{\lambda} \nabla_t \varphi - \mathbf{k} \wedge \frac{1}{\lambda}\frac{\partial \varphi}{\partial t} \nabla t.$$

Apparently the remaining contribution to the actual wind consists of a term, which involves the product of the geopotential tendency and the reciprocal speed of propagation of the isochronals.

Since the velocity of propagation has been adjusted to, say, the true air speed c, the magnitude of this contribution is approximately equal to $\frac{1}{\lambda c}\frac{\partial \varphi}{\partial t}$.

Table I gives this quantity at 50° N in terms of the geopotential tendency expressed in geopotential meters per hour and the true air speed in knots.

TABLE I

TAS knots / tendency $gpm.hr^{-1}$	200	250	300	350	400	450	500
0	0	0	0	0	0	0	0
8	3.6	2.9	2.4	2.0	1.8	1.6	1.4
16	7.2	5.8	4.8	4.1	3.6	3.2	2.8
24	10.8	8.7	7.2	6.1	5.4	4.8	4.3
		turbo prop (250–350)			turbo jet (400–500)		
	piston-engined (200–300)						

Taking into account the velocity intervals for piston-engined, turbo prop and turbo jet aircraft we may notice that for turbo prop and turbo jet powered aircraft the velocity correction amounts to less than 10 knots, even for very high tendency values. As accuracy of the forecast wind of 10 knots is difficult to obtain, it is justified in practice to use a composite topography only instead of the composite topography with geostrophic flow. For piston-engined aircraft the velocity correction may circumstantially amount to more than 10 knots. Then it is useful to pay attention to those chart areas where the upper air flow is subject to fast alterations in time.

6. Theory of single heading flights

Single heading navigation or constant drift course is a simple system of navigation which generally saves flight time and fuel. The preparation of the flight and the work to be done in the cockpit are reduced to a minimum. Apart from that the theory is of importance in the calculation of the track of pilotless aircraft.

The system has been studied mainly for flights that are conducted on isobaric surfaces and quasi-horizontal flight levels. The theory that is most often expressed by the well-known drift formula of Bellamy [1943], has succesfully been applied to piston-engined air traffic in middle and high latitudes. However, the development of turbo prop and turbo jet powered aircraft demands an extension of the theory, since long range operations with these aircraft are performed on sloping surfaces which deviate considerably from the horizontal.

This theory will be reviewed here, taking into account the variability of the airflow in space and time.

Single heading navigation is based on the principle that the angle between the axis of the aircraft and a fixed line of reference in a rectangular coordinate system does not change along the track, allowing the airplane to drift freely with the wind.

This may be expressed mathematically by the equation

$$\frac{d\delta}{dt} = 0 \qquad \text{(IV.1)}$$

where δ, the *grid heading* refers to the above defined drift-correction angle, taken with respect to the straight line on the chart between point of departure and destination. The coordinate system is superimposed on a current conformal chart projection like the cylindrical Mercator, Lambert conformal conic or polar stereographic projection. Only on the Mercator chart the grid heading will be the true heading.

We restrict our investigations to those chart areas, where the scale factor of the chart is approximately equal to unity and the variation of the scale is assumed to be very small. In practice the change of the true air speed may be neglected, not only for quasi-horizontal flights but also for the continuous or stepped climb associated with turbo prop and jet operations.

The concepts of geostrophic approximation and geostrophic flow play a dominant part in the theory. The well-known drift equation of Bellamy for instance is based on these objectives.

A single heading flight conducted on an isobaric surface is defined by the equations

$$\frac{d\delta}{dt} = 0, \quad \frac{dp}{dt} = 0.$$

Here the drift equation of Bellamy expresses a relationship between the grid heading δ, the true air speed c, the chart distance d and the geopotential difference between the points of departure and destination (fig. 9), according to the formula

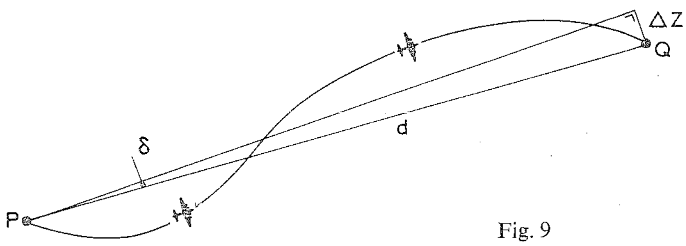

Fig. 9

$$\sin \delta = \frac{1}{\lambda} \frac{\varphi(Q) - \varphi(P)}{cd} \tag{IV.2}$$

If c is expressed in knots, d in nautical miles and true height z in feet, (IV.2) may be written

$$\sin \delta = \frac{21.47}{\sin L_m} \frac{z(Q) - z(P)}{cd},$$

where L_m represents the mean latitude along the track. It is worth noting that the grid heading is apparently independent of the structure of the airflow, because it is determined by the geopotential values in the endpoints. This property is lost in arbitrary surfaces and non-stationary wind fields.

In quasi horizontal flight levels the equation is usually quoted in the form

$$\sin \delta \cong \kappa \frac{D(Q) - D(P)}{cd}, \tag{IV.3}$$

$$\kappa = \frac{g}{\lambda},$$

where the D-value represents the "altimeter correction".

The *altimeter correction* D at any point at which the pressure is p, is defined as the difference between the true height z of the point and the height z_p in the standard I.C.A.N. atmosphere at which the pressure p occurs,

$$D = z - z_p = \frac{1}{g}(\varphi - \varphi_s) \tag{IV.4}$$

where φ_s denotes the geopotential in the standard atmosphere. The true height is measured by means of a *radio-radar altimeter*, the height in the standard atmosphere by the *pressure altimeter*, calibrated according to the (I.C.A.N.) standard atmosphere, where its subscale is set to a sea level pressure of 1013.2 mb.

Apart from the drift angle, it is customary in practice to consider the *total displacement* $\triangle$ Z.

Referring to fig. 9 we have

$$\triangle Z = d \sin \delta$$

or, on account of (IV.2) and (IV.3)

$$\triangle Z = \frac{1}{\lambda} \frac{\varphi(Q) - \varphi(P)}{c} \cong \kappa \frac{D(Q) - D(P)}{c}. \tag{IV.5}$$

It follows from this equation that the total displacement is inversely proportional to the true air speed. As the true air speed of turbo prop and jet aircraft is approximately twice that for piston-engined aircraft, the corresponding total displacement is reduced with a factor two.

A single heading flight may be conducted on an isobaric surface with the aid of a constant reading of the pressure altimeter. Keeping a constant reading of other instruments, the flight proceeds within other surfaces. For instance, a constant reading of the radio-radar altimeter results in a flight within a geopotential surface, a constant reading of a thermometer leads to a flight in an isothermal surface etc. Within certain limits the drift equation (IV.4) applies for single heading flights within such surfaces, but it is obvious that the exact equation (IV.2) should be adjusted to these special flights. In order to derive the subsequent equations we make use of the concept of geostrophic flow in space and time.

Before going into detail we summarize briefly a demonstration of Bellamy's equation which is rather based on the concept of geostrophic flow, de Jong [1956].

The true air speed vector along the track is characterized by a constant magnitude and constant direction. Consequently we may introduce a scalar pattern defined by a stream function φ', for which

$$\mathbf{c} = \mathbf{k} \wedge \frac{1}{\lambda} \nabla \varphi' . \tag{IV.6}$$

The scalar pattern consists of a set of parallel equidistant straight lines $\varphi' =$ const. (fig. 10). The ground speed vector $\mathbf{g}$ along the track is the vector

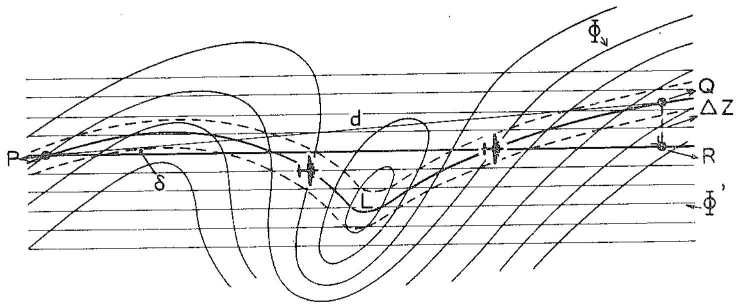

Fig. 10

sum of the true air speed vector $\mathbf{c}$ and wind vector $\mathbf{v}$. Thus

$$\mathbf{g} = \mathbf{c} + \mathbf{v}$$

In virtue of (I.4) and (IV.6) we have

$$\mathbf{g} = \mathbf{k} \wedge \frac{1}{\lambda} \nabla_p \varphi + \mathbf{k} \wedge \frac{1}{\lambda} \nabla \varphi'$$

$$\text{or} \qquad \mathbf{g} = \mathbf{k} \wedge \frac{1}{\lambda} \nabla_p (\varphi + \varphi'),$$

showing that the vector field g possesses a stream function $\varphi + \varphi'$. The vector lines in the g field represent single heading trajectories. We then find the remarkable result, that a graphical addition of the scalar patterns $\varphi =$ const. and $\varphi' =$ const. yields a pattern of single heading tracks. The ground speed along the track is inversely proportional to the distance of neighbouring single heading tracks.

Let P and Q be located at one of these tracks, then we have according to the graphical addition

$$\varphi(Q) + \varphi'(Q) = \varphi(P) + \varphi'(P).$$

But in view of the definition of φ' we may write

$$\frac{\varphi'(P) - \varphi'(Q)}{\lambda c} = \overline{QR} = d \sin \delta,$$

where $\overline{QR}$ is the total displacement $\triangle$ Z defined by (IV.5). Therefore

$$\sin \delta = \frac{1}{\lambda} \frac{\varphi(Q) - \varphi(P)}{cd},$$

resulting in the drift equation of Bellamy.

The above demonstration involves a very quick and elegant method to construct a single heading track between point of departure and destination (see fig. 10). For this purpose one draws a set of parallel equidistant straight lines on a transparent sheet of paper. Introducing the stream function φ', this function φ' is labelled in such a way that the increment $\triangle \varphi'$ is equal to the increment $\triangle \varphi$ of the geopotential in the pressure contour chart. Besides, the distance between the straight lines is such that the "geostrophic wind" in the auxiliary chart equals the true air speed c. The auxiliary chart is put on a light table and the pressure contour chart is placed upon the sheet and rotated until the sum of φ and φ' in the point of departure P is equal to the sum of φ and φ' at destination Q. Both charts being in the right position, the track can be drawn by connecting the points of intersection of φ and φ'-lines. This addition method can be carried out in a few minutes.

6.1. Single heading flights in non-stationary isobaric flow

When the airflow in an isobaric surface is subject to fast alterations with respect to the total flight time we may embed the single heading track within a composite topography with geostrophic flow (fig. 11), as has been shown in part IV, section 2.

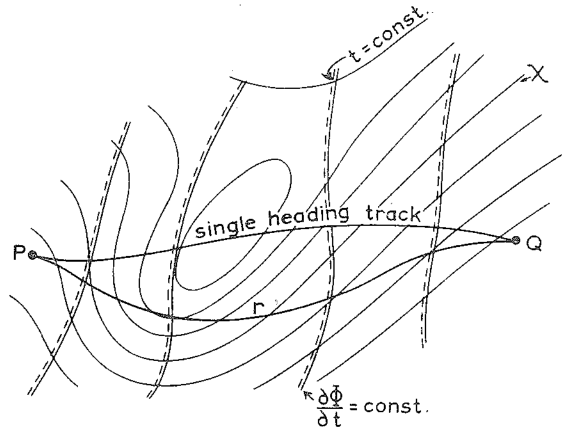

Fig. 11

The stream function associated with this composite topography is, according to (II.6)

$$\chi = (\varphi + \varphi^*)_t,$$

where the time function $t = t(x, y)$ is determined by the relation

$$\frac{\partial \varphi}{\partial t} = - \frac{d\varphi^*}{dt} \tag{IV.7}$$

The time function has been specified by selecting $\varphi^*(t)$, in such a way that it indicates the right progress of the flight.

Then the drift equation (IV.2) becomes

$$\sin \delta = \frac{1}{\lambda} \frac{\chi(Q) - \chi(P)}{cd}$$

$$= \frac{1}{\lambda} \frac{\varphi\big(t(Q)\big) - \varphi\big(t(P)\big) + \varphi^*\big(t(Q)\big) - \varphi^*\big(t(P)\big)}{cd}$$

In the composite topography we consider an arbitrary curve r and integrate (IV.7) with respect to t along this curve

$$\int_{t(P)}^{t(Q)} (r) \frac{d\varphi^*}{dt} dt = - \int_{t(P)}^{t(Q)} (r) \frac{\partial \varphi}{\partial t} dt.$$

As φ^* depends only on t, we get

$$\varphi^*(t(Q)) - \varphi^*(t(P)) = - \int_{t(P)}^{t(Q)} (r) \frac{\partial \varphi}{\partial t} dt.$$

Especially, by taking for r the single heading track itself, we obtain

$$\boxed{\sin \delta = \frac{1}{\lambda} \frac{\varphi(t(Q)) - \varphi(t(P)) - \int_{t(P)}^{t(Q)} \frac{\partial \varphi}{\partial t} dt.}{cd}} \qquad \text{(IV.8)}$$

The result states that the drift correction angle not only depends on the end values of the isobaric geopotential, but involves in addition a line integral of the geopotential tendency. It is noteworthy that the line integral can be evaluated along any curve joining the point of departure and destination, provided that the integration is performed in the specified composite topography. Furthermore, it is clear that the handsome graphical addition method for the construction of the track still holds.

6.2. Single heading flights within stationary flow in arbitrary surfaces

We proceed by studying single heading fligths in arbitrary surfaces within stationary or quasi-stationary airflow.

In part IV, section 3 it has been proved that the single heading track can be embedded in a surface with geostrophic flow.

The drift equation may therefore be derived by the application of a method similar to that in the previous section.

In a surface with geostrophic flow we have according to formula (IV.2)

$$\sin \delta = \frac{1}{\lambda} \frac{\psi(Q) - \psi(P)}{cd},$$

where $\psi = \varphi - \varphi_{S_0}$.

Hence

$$\sin \delta = \frac{1}{\lambda} \frac{\varphi(Q) - \varphi(P) - \varphi_{S_0}(Q) + \varphi_{S_0}(P)}{cd}$$

S_0 denotes the scalar value for the specified surface under consideration.

In virtue of the meaning of φ_{S_0}, cf. (I.17)

$$\varphi_{S_0}(Q) - \varphi_{S_0}(P) = \int_{p(P)}^{p(Q)} \frac{1}{\rho(p, S_0)} dp. \tag{IV.9}$$

Since the single heading track is embedded in the surface $S = S_0$, the density $\rho(p, S_0)$ is to be interpreted as the density along the track itself.

In view of the gas equation (I.12) the drift equation finally becomes

$$\boxed{\sin \delta = \frac{1}{\lambda} \frac{\varphi(Q) - \varphi(P) + \int_{p(P)}^{p(Q)} RT \, d \ln p}{cd}} \tag{IV.10}$$

The integration may be performed along each curve joining P and Q, provided that this curve is located on the scalar surface $S = S_0$.

Apparently the grid heading involves an integral which may be understood as *the "thickness" of a layer where the temperature-density distribution corresponds to that along the track.*

When $\bar{T}$ represents the mean (virtual) temperature along the track, the drift equation (IV.10) may be written

$$\sin \delta = \frac{1}{\lambda} \frac{\varphi(Q) - \varphi(P) + R\bar{T} \ln p(Q) / p(P)}{cd} \tag{IV.11}$$

The result offers some interesting interpretations. On an isobaric surface we have p(P) = p(Q). Then we have to deal with the drift equation of Bellamy.

A single heading flight in a *geopotential surface* is characterized by $\varphi(P) = \varphi(Q)$ Here the drift equation takes the form

$$\sin \delta = \frac{1}{\lambda} \frac{R\bar{T}}{cd} \ln p(P) \,/\, p(Q) \tag{IV.12}$$

When the pressure-temperature distribution along the track corresponds to that of the standard atmosphere, then the second term in the numerator reduces to the geopotential difference $\varphi_s(P) - \varphi_s(Q)$ in the standard atmosphere. Consequently equation (IV.10) may be written

$$\sin \delta = \frac{1}{\lambda} \frac{\varphi(Q)) - \varphi_s(Q) + \varphi(P) - \varphi_s(P)}{cd} .$$

In virtue of the definition of the D-value, (cf. IV.4)

$$D(Q) = \frac{1}{g}\big(\varphi(Q) - \varphi_s(Q)\big),$$

$$D(P) = \frac{1}{g}\big(\varphi(P) - \varphi_s(P)\big),$$

we obtain

$$\sin \delta = \kappa \frac{D(Q) - D(P)}{cd}, \; \kappa = \frac{g}{\lambda} \tag{IV.13}$$

The same result is found, when the *mean* temperature $\bar{T}$ happens to be equal to the mean temperature in the (I.C.A.N.) standard atmosphere between the layers p (P) and p (Q).

The above condition is far from being realised in practice as well for flights with turbo prop and turbo jet aircraft as for quasi horizontal flights with piston-engined aircraft. Therefore the drift equation (IV.3) should be interpreted with care.

When single heading flights are conducted on ordinary physical surfaces, e.g. on isothermal surfaces, the pressure-temperature distribution along the track is known beforehand. Then it suffices to replace φ in the drift equation (IV.2) by the stream function ψ associated with these surfaces cf. (I.18).

Referring to the theory outlined in part I we may discus this substitution more in detail.

Single heading flight in polytropic surfaces. These are characterized by a conservation of the drift correction angle δ and scalar $S = p\rho^{-k}$:

$$\frac{d\delta}{dt} = 0, \quad \frac{dS}{dt} = 0.$$

The corresponding drift equation becomes, in virtue of the geostrophic wind equation (I.25)

$$\sin\delta = \frac{1}{\lambda}\,\frac{\varphi(Q) - \varphi(P) + \dfrac{k}{k-1} R\bigl(T(Q) - T(P)\bigr)}{cd} \tag{IV.14}$$

φ and T refer to the surface geopotential respectively surface temperature distribution.

For specified values of k we obtain the expressions for isobaric, isothermal, isosteric and isentropic surfaces.

Isobaric surfaces

We have
$$\frac{d\delta}{dt} = 0, \frac{dp}{dt} = 0.$$

The drift equation becomes (Bellamy)

$$\sin\delta = \frac{1}{\lambda}\,\frac{\varphi(Q) - \varphi(P)}{cd}$$

Isothermal surfaces

The single heading flight is defined by

$$\frac{d\delta}{dt} = 0, \frac{dT}{dt} = 0.$$

In view of (I.26) the drift equation becomes

$$\sin\delta = \frac{1}{\lambda}\,\frac{\varphi(Q) - \varphi(P) + RT \ln p(Q)/p(P)}{cd}. \tag{IV.15}$$

Isosteric surfaces

Now $$\frac{d\delta}{dt} = 0, \frac{d\rho}{dt} = 0$$

and the drift equation takes the form, cf. (I.27),

$$\sin\delta = \frac{1}{\lambda}\,\frac{\varphi(Q) - \varphi(P) + R\big(T(Q) - T(P)\big).}{cd} \qquad \text{(IV.16)}$$

Isentropic surfaces

Here we have $$\frac{d\delta}{dt} = 0, \frac{d\Theta}{dt} = 0.$$

On account of formula (I.6) the expression for the grid heading becomes

$$\sin\delta = \frac{1}{\lambda}\,\frac{\varphi(Q) - \varphi(P) + c_p\big(T(Q) - T(P)\big)}{cd} \qquad \text{(IV.17)}$$

It is of importance to observe that the formulae for single heading flights within these physical surfaces give the grid heading independent of the wind distribution along the track, just like in isobaric surfaces. The grid heading δ may be computed easily from the geopotential and temperature or pressure data in the point of departure and destination. These end values may be read from the subsequent upper air charts. Besides, the construction of the track, by means of the graphical addition of two scalar patterns, which has been outlined in section 6 for isobaric surfaces may be transferred without alterations to the above single heading flights in polytropic surfaces.

6.3. Single heading flight within non-stationary airflow in general

We now discuss the problem within non-stationary airflow. It was proved in section 3 that every pressure pattern track may be embedded within a geostrophic motion. In particular this property holds for any single heading track in space. Let r be the track between the points P and Q. Then we may add a uniquely defined geostrophic configuration, for which the space function $p = p(x, y)$ and time function $t = t(x, y)$ indicate the actual pressure distribution and progress of flight along the track. According to (III.5) the stream function, associated with the geostrophic motion becomes

$$\mathfrak{z} = (\varphi + \varphi^*)_{p,t} + (\chi^*)_p,$$

$$\varphi^* = \varphi^*(t, p), \chi^* = \chi^*(p),$$

where the space function is determined by the relation

$$\frac{\partial \chi}{\partial p} = -\frac{d\chi^*}{dp}, \tag{IV. 18}$$

$$\chi = (\varphi + \varphi^*)_t \tag{IV.19}$$

and the time function by

$$\frac{\partial \varphi}{\partial t} = -\frac{\partial \varphi^*}{\partial t}, \tag{IV.20}$$

$$t = t\big(x, y, p(x, y)\big).$$

The arbitrary functions φ^* and χ^* has been specified in such a manner that the resulting geostrophic motion fulfils the conditions along the track, quoted above.

For the drift equation (IV.2) we get

$$\sin \delta = \frac{1}{\lambda} \frac{\mathfrak{z}(Q) - \mathfrak{z}(P)}{cd}$$

or

$$\sin \delta = \frac{1}{\lambda} \left(\frac{\varphi\big(t(Q), p(Q)\big) - \varphi\big(t(P), p(P)\big) + \varphi^*\big(t(Q), p(Q)\big)}{cd} \right. \\ \left. \frac{- \varphi^*\big(t(P), p(P)\big) + \chi^*\big(p(Q)\big) - \chi^*\big(p(P)\big)}{cd} \right) \tag{IV.21}$$

In the geostrophic approximation we consider an arbitrary curve r and integrate (IV.18) with respect to p along this curve

$$\int_{p(P)}^{p(Q)} (r) \frac{d\chi^*}{dp} dp = - \int_{p(P)}^{p(Q)} (r) \frac{\partial \chi}{\partial p} dp.$$

Hence

$$\chi^*(p(Q)) - \chi^*(p(P)) = - \int_{p(P)}^{p(Q)} (r)\ \frac{\partial \chi}{\partial p}\, dp. \tag{IV.22}$$

In view of (IV.19) we may remark that

$$\frac{\partial \chi}{\partial p} = \frac{\partial \varphi}{\partial p} + \frac{\partial \varphi}{\partial t}\frac{\partial t}{\partial p} + \frac{\partial \varphi^*}{\partial p} + \frac{\partial \varphi^*}{\partial t}\frac{\partial t}{\partial p}.$$

But by (IV.20) this reduces to

$$\frac{\partial \chi}{\partial p} = \frac{\partial \varphi}{\partial p} + \frac{\partial \varphi^*}{\partial p}.$$

Therefore the term on the right side of (IV.22) becomes

$$- \int_{p(P)}^{p(Q)} (r)\ \frac{\partial \varphi}{\partial p}\, dp - \int_{p(P)}^{p(Q)} (r)\ \frac{\partial \varphi^*}{\partial p}\, dp = \int_{p(P)}^{p(Q)} (r)\ \frac{dp}{\rho} - \int_{p(P)}^{p(Q)} (r)\ \frac{\partial \varphi^*}{\partial p}\, dp.$$

Now, according to the definition of φ^*, we observe that

$$d\varphi^* = \frac{\partial \varphi^*}{\partial t}\, dt + \frac{\partial \varphi^*}{\partial p}\, dp,$$

whence

$$\int_{p(P)}^{p(Q)} (r)\ \frac{\partial \varphi^*}{\partial p}\, dp = \varphi^*(t(Q), p(Q)) - \varphi^*(t(P), p(P)) - \int_{t(P)}^{t(Q)} (r)\ \frac{\partial \varphi^*}{\partial t}\, dt.$$

Thus (IV.22) may be written, in view of (IV.20) (identifying r with the single heading track):

$$\chi^*(p(Q)) - \chi^*(p(P)) = \varphi^*(t(P), p(P)) - \varphi^*(t(Q), p(Q)) + \int_{p(P)}^{p(Q)} \frac{dp}{\rho} - \int_{t(P)}^{t(Q)} \frac{\partial \varphi}{\partial t}\, dt.$$

By substituting this expression in (IV.21), we finally obtain

$$\sin\delta = \frac{1}{\lambda}\,\frac{\varphi\big(t(Q), p(Q)\big) - \varphi\big(t(P), p(P)\big) + \int\limits_{p(P)}^{p(Q)} \frac{dp}{\rho} - \int\limits_{t(P)}^{t(Q)} \frac{\partial\varphi}{\partial t}\,dt.}{cd} \tag{IV.23}$$

The grid heading involves two line integrals. The first consisting of the "thickness"

$$\int\limits_{p(P)}^{p(Q)} \frac{dp}{\rho} = \int\limits_{p(P)}^{p(Q)} RT\,d\ln p$$

associated with the *composite pressure-temperature distribution along* the track. The second gives an integral of the geopotential tendency.

Again, it is noteworthy that the line integrals may be evaluated along each track in the geostrophic motion, joining the point of departure and destination.

As a special case flights may be performed in scalar surfaces $S = S_o = \text{const.}$ with time dependent geostrophic flow, e.g. in isothermal surfaces. Then the drift equation reduces to

$$\sin\delta = \frac{1}{\lambda}\,\frac{\psi\big(t(Q)\big) - \psi\big(t(P)\big) - \int\limits_{t(P)}^{t(Q)} \frac{\partial\psi}{\partial t}\,dt,}{cd} \tag{IV.24}$$

similar to the result for flights in non-stationary isobaric surfaces.

This may be demonstrated as follows:

In (IV.23) the first line integral becomes

$$\int\limits_{p(P)}^{p(Q)} \frac{dp}{\rho} = \int\limits_{p(P)}^{p(Q)} \frac{dp}{\rho(p, S_o)} = \int\limits_{p(P)}^{p_o} \frac{dp}{\rho(p, S_o)} + \int\limits_{p_o}^{p(Q)} \frac{dp}{\rho(p, S_o)},$$

where p_o represents an arbitrary reference pressure level. By definition of (I.17) this may be written

$$\int\limits_{p(P)}^{p(Q)} \frac{dp}{\rho} = \varphi_{S_o}\big(p(P)\big) - \varphi_{S_o}\big(p(Q)\big), \text{ independent of time}$$

Thus we get for the numerator of (IV.23)

$$\varphi\big(t(Q), p(Q)\big) - \varphi_{S_0}\big(p(Q)\big) - \varphi\big(t(P), p(P)\big) + \varphi_{S_0}\big(p(P)\big) - \int\limits_{t(P)}^{t(Q)} \frac{\partial \varphi}{\partial t}\, dt$$

According to the geostrophic wind equation (I.18) the stream function ψ, associated with a surface with geostrophic flow, is

$$\psi = \varphi - \varphi_{S_0}.$$

So that the numerator becomes

$$\psi\big(t(Q)\big) - \psi\big(t(P)\big) - \int\limits_{t(P)}^{t(Q)} \frac{\partial \varphi}{\partial t}\, dt$$

Differentiation of ψ with respect to time yields

$$\frac{\partial \psi}{\partial t} = \frac{\partial \varphi}{\partial p}\frac{\partial p}{\partial t} + \frac{\partial \varphi}{\partial t} - \frac{\partial \varphi_{S_0}}{\partial p}\frac{\partial p}{\partial t}.$$

But in virtue of (I.17)

$$\frac{\partial \varphi_{S_0}}{\partial p} = -\frac{1}{\rho(p, S_0)}$$

and so on account of (I.11) we have

$$\frac{\partial \varphi}{\partial p} = \frac{\partial \varphi_{S_0}}{\partial p},$$

whence

$$\frac{\partial \psi}{\partial t} = \frac{\partial \varphi}{\partial t}.$$

Substituting for $\dfrac{\partial \varphi}{\partial t}$ in the last integral in the numerator of the drift equation we get

$$\sin \delta = \frac{1}{\lambda} \frac{\psi\big(t(Q)\big) - \psi\big(t(P)\big) - \int\limits_{t(P)}^{t(Q)} \frac{\partial \psi}{\partial t}\, dt.}{cd}$$

To complete this survey we may remark that if the composite pressure-temperature distribution along the track happens to correspond to the pressure-temperature distribution in the (I.C.A.N.) standard atmosphere, then the drift equation reduces to

$$\sin \delta = \kappa \frac{D(Q) - D(P) - \int\limits_{t(P)}^{t(Q)} \frac{\partial D}{\partial t}\, dt.}{cd} \tag{IV.25}$$

where D represents the "altimeter correction".

In a *geopotential surface* we have $\varphi\big(t(P), p(P)\big) = \varphi\big(t(Q), p(Q)\big)$
Then

$$\sin \delta = \frac{1}{\lambda} \frac{\int\limits_{p(P)}^{p(Q)} \frac{dp}{\rho} - \int\limits_{t(P)}^{t(Q)} \frac{\partial \varphi}{\partial t}\, dt.}{cd}$$

Finally we observe that the expressions reduce to those given in the previous sections, if either $t =$ constant or $p =$ constant.

In turbo prop and turbo jet operations a most economical flight at cruising level is obtained by application of a continuous climb or drift up system. The optimum flight level increases during the flight depending on gross weight, fuel consumption, temperature and other factors. By air traffic control requirements the continuous cruising climb may be replaced by a stepped cruise system, the number of steps are determined by engine performance and height of steps. Figure 12 shows some of the flight characteristics.

In general turbo prop aircraft operate to a height of 11.000 m, turbo jet aircraft to a height of 14,000 m. Since on the one hand the flight characteristics depend on the type of aircraft and on the other hand the conditions which a flight analysis has to fulfil are difficult to realise in practice, we must proceed somewhat schematically.

A. First we will examine a fictitious single heading flight Amsterdam–Vancouver with a Britannia turbo prop. The top of climb is between 18,000 and 25,000 ft, the top of descent between 30,000 and 35,000 ft. Thus it is evident, that we have to consult 500, 400 and 300 mb upper air data. We have chosen a date on which the wind structure may be considered to be

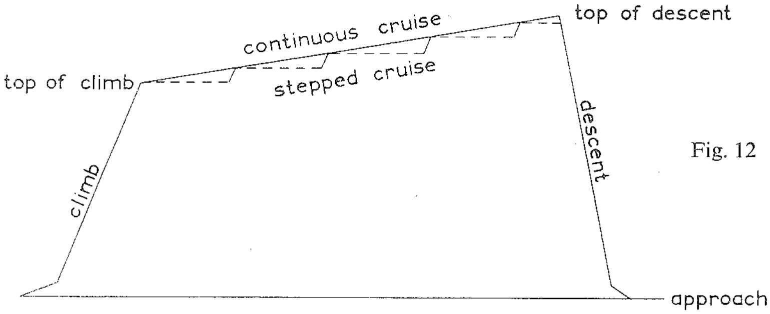

Fig. 12

quasi-stationary with regard to the total flight endurance (approximately 13 hours). The true air speed is nearby 300 kn.

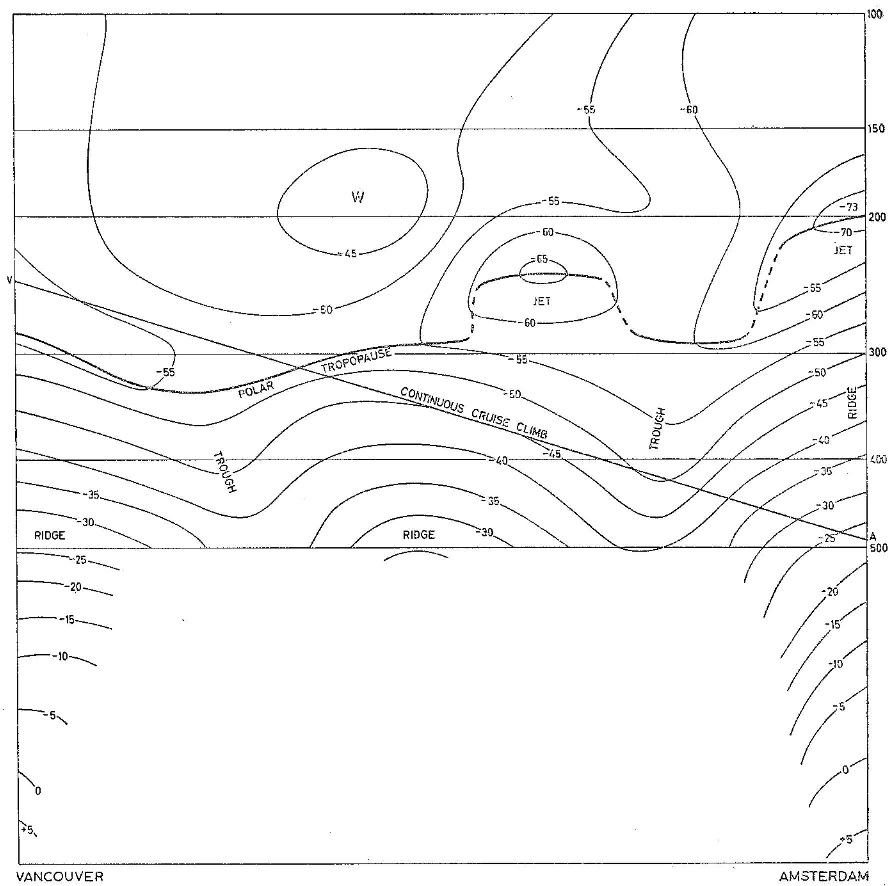

Fig. 13

Figure 13 shows a cross-section of the temperature distribution with insertion of the cruise climb AV. This cross section has been prepared by inspection of all available upper air observations in the vicinity of the track. As in practice the flight level is very sensitive with respect to the on route temperatures the indicated flight course is drawn rather schematically.

The temperature pressure distribution along AV has been transferred from the cross section to an aerological diagram (T-ln p diagram), climb and descent included, as well as the I.C.A.N. standard atmosphere (fig. 14).

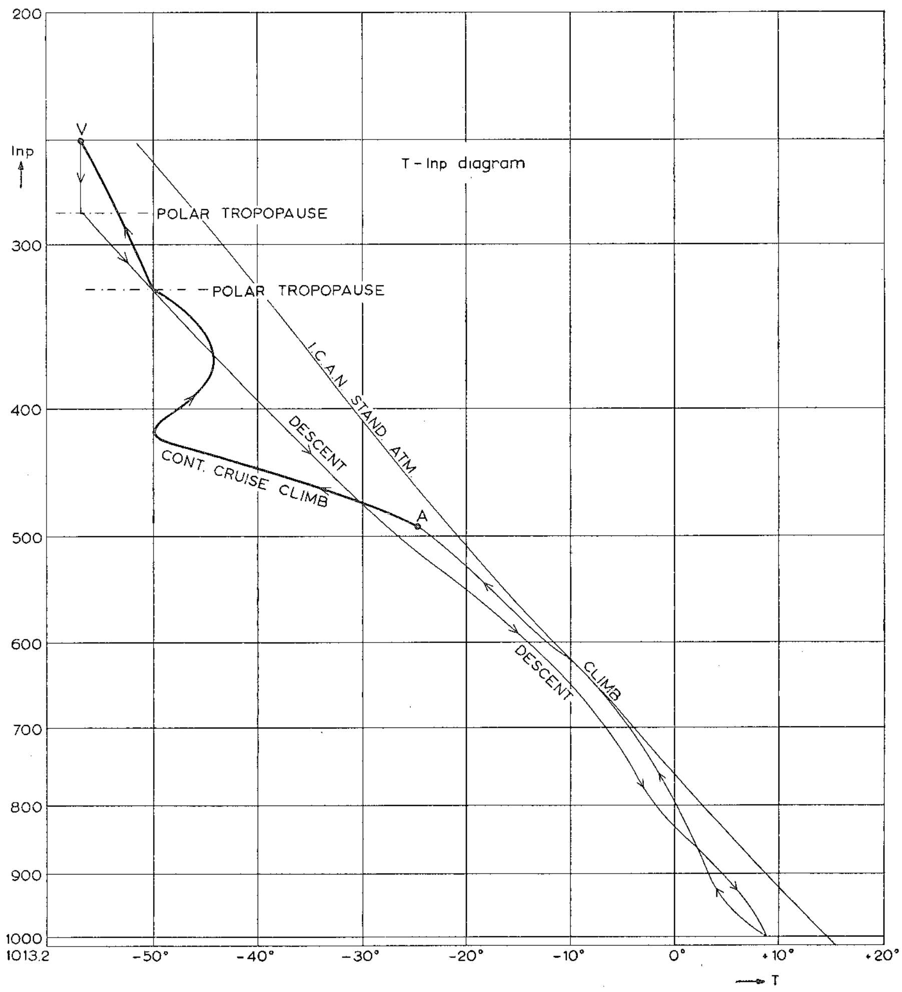

Fig. 14

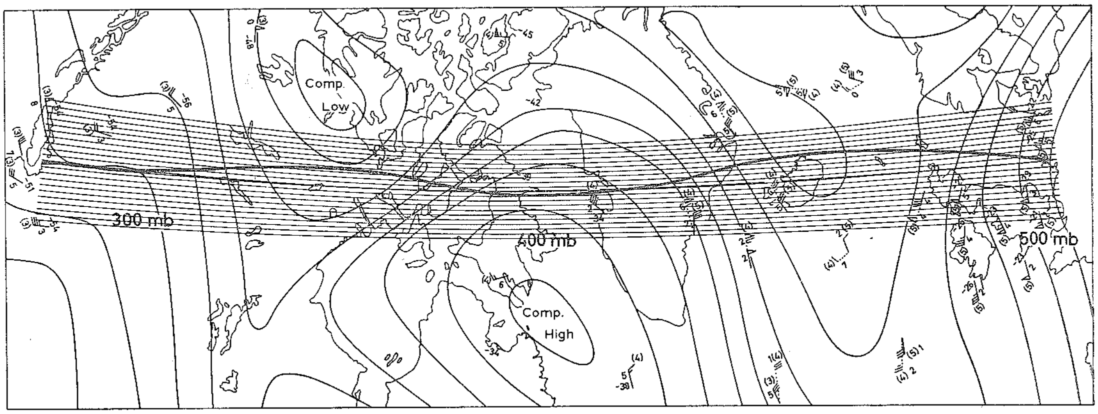

CHART IX. Composite chart in space adjusted to a continuous cruise climb for a flight Amsterdam–Vancouver with a Bristol Britannia (turbo prop). Date 2 Febr. 1958, 00.00 G.M.T. Increment for stream lines in both patterns is 80 gpm. Upper wind data are shown in conventional fashion. Numbers in brackets above wind data refer to the pressure level, for which the wind applies.

Chart IX represents a composite chart in space which has been adjusted to the continuous cruising climb. In order to interpret geostrophic motion within this chart, it involves a portion of the 500 mb analysis in the eastern part and a portion of the 300 mb analysis in the western part of the chart area. Halfway on the track the 400 mb analysis has been copied. In the remaining sections the stream lines have been drawn by free-hand extrapolation applying some smoothing and by consultation of 500 — 400 mb and 400 — 300 mb data. The resulting stream lines are no longer contour lines, but represent isopleths of a stream function for the special composite chart with an increment of 80 gpm.

To construct the single heading track by means of the addition method another set of stream lines has been drawn which determines the true air speed vector distribution. Instead of straight parallel lines a pattern of curved lines has been drawn, mainly to incorporate the special features of the chart's projection. (polar stereographic). The great circle Amsterdam–Vancouver serves as base-line and the gradient in the stream line pattern determines a true air speed of 300 kn. The increment in the stream line pattern is again 80 gpm.

The pattern has been superimposed on the composite chart in such a manner that the algebraic sum of both stream functions in the point of departure is equal to that in destination. The curve joining the points of intersection of both patterns is the single heading track.

By its location within the "long waves" the track shows an undulatory character. The total displacement, however, is small. We will calculate the displacement by using different expressions, which have been derived in the previous sections.

The most exact value is found by using formula (IV.10)

$$\triangle Z = \frac{1}{\lambda} \frac{\varphi(V) - \varphi(A) + \int_A^V RT \, d \ln p.}{c}$$

From the (T- ln p diagram) a "thickness" may be derived between A and V of 4,464 gpm. Further one finds

$$\varphi(A) = 5{,}620 \text{ gpm}$$

$$\varphi(V) = 10{,}100 \text{ gpm}$$

so that with $L_m = 65°N$, $c = 300$ kn and 1 gpm = 3.28 ft.

$$\triangle Z = \frac{21.47}{0.96} \frac{(10{,}100 - 5{,}620 - 4{,}464)3.28}{300} = 0.24 \,.\, 16 \simeq 4 \text{ n.m.}$$

a total displacement of approximately 4 n.m. to the south.

When we compute the displacement by merely reading the difference of values of the stream functions at the end points in the composite chart, we have

$$\chi(V) - \chi(A) = 20 \text{ gpm}$$

$$\triangle Z = 0.24 \,.\, 20 \simeq 5 \text{ n.m.}$$

in good agreement with the exact value.

Next we may determine an approximate value for the displacement by taking the D-value expression (IV.13).

With D(A) in gpm $= \varphi(A) - \varphi(\text{I.C.A.N.}) = 5{,}620 - 5{,}723 = -103$ gpm

D(V) in gpm $= \varphi(V) - \varphi(\text{I.C.A.N.}) = 10{,}100 - 10{,}363 = -263$ gpm

a displacement

$\triangle Z = 0.24(-103 - (-263)) = 0.24 \,.\, 160 \sim 39$ n.m. results.

Besides, we may find an approximate value for the displacement by examination of the 500 mb chart and 300 mb chart separately.

Then we have to use equation (IV.2).

Here $\varphi(A) = 5{,}480$ gpm

$\varphi(V) = 5.430$ gpm

whence $\triangle Z = 0.24.(5{,}430 - 5.480) = -0.24 \,.\, 50 \simeq -12$ n.m. a displacement of 12 n.m. to the north.

In the 300 mb chart $\varphi(A) = 9{,}000$ gpm

$\varphi(V) = 8{,}900$ gpm

and $\triangle Z = 0.24.(8{,}900 - 9{,}000) = -0.24 \,.\, 100 \simeq -24$ n.m. resulting in a displacement of 24 n.m. to the north.

The above computations of the total displacement justify the statement that the commonly used formulae of Bellamy may indeed give erroneous results, when flights with turbo prop and turbo jet powered aircraft are considered.

B. Next we will consider a single heading flight New York–Amsterdam with a Douglas D.C. 8.

As in example A we consider a fictitious flight between both stations. In addition we have to make some assumptions concerning the characteristics of this jet flight. The top of climb is about 30,000 ft, the top of descent around 40,000 ft. Here it will be advisable to study 200, 250 and 300 mb data. The true air speed is approximately 470 kn. Consequently, the flight time New York–Amsterdam amounts to 6 à 7 hours. If a stepped climb system is applied the number of steps does not surpass two steps of 4000 feet each. Due to the short flight time the upper air flow may most often be considered to be quasi-stationary for these jet aircraft, but to demonstrate the theory more clearly we have selected a situation which shows high tendency values (more than 20 gpm hr^{-1} near the British Isles). The flight has

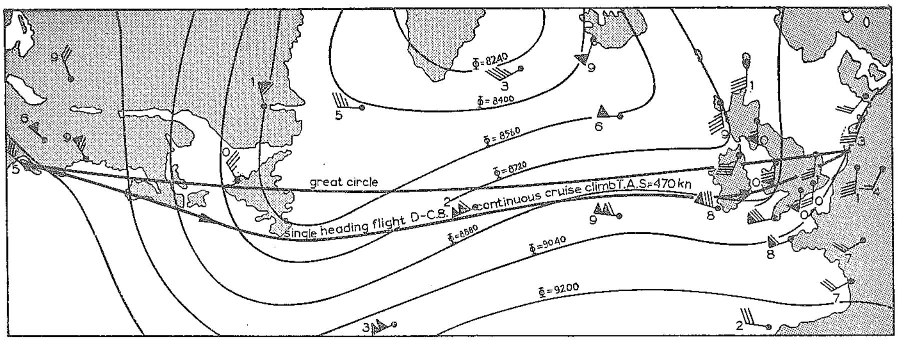

CHART X. 300 mb analysis valid for 18 Dec. 1957, 12.00 G.M.T. Upper wind data are shown as usual. Increment of geopotential φ is 160 gpm.

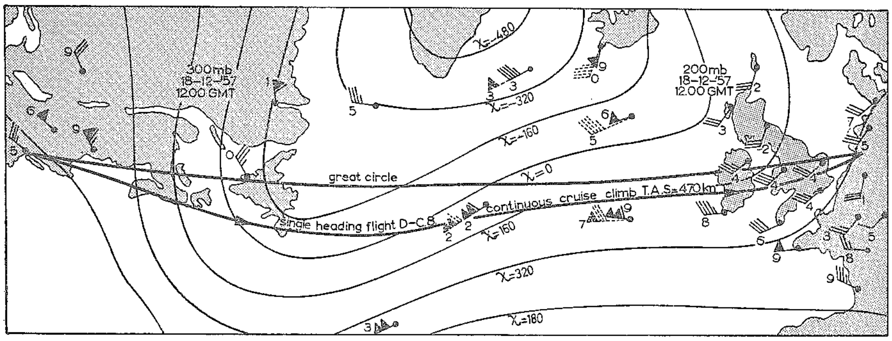

CHART XI. Composite chart in space valid for 18 Dec. 1957, 12.00 G.M.T. Wind data are plotted in conventional fashion. Where two wind data appear, the broken line symbol refers to the 200 mb pressure level, the solid one to the 300 mb pressure level. The increment of the stream lines χ = const. is 160 gpm.

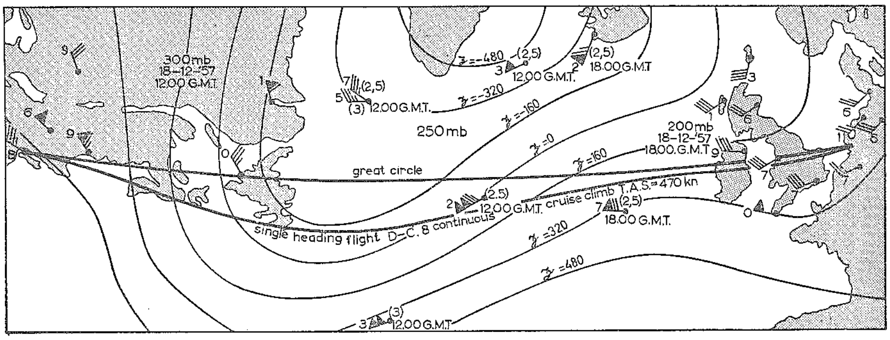

CHART XII. Composite chart in space and time valid for 18 Dec. 1957, 12.00 G.M.T. – 18 Dec. 1957, 18.00 G.M.T. Wind data as usual, numbers in brackets refer to 200-, 250- and 300 mb pressure levels. The increment of the stream lines $\mathfrak{z}$ = const. is 160 gpm.

been studied in a fixed time isobaric chart, in a composite chart in space and a composite chart in space and time. Chart X valid for 18 Dec. 1957 12.00 G.M.T. is a reproduction of the 300 mb chart with wind data plotted in convential fashion for upper air map times. The contour lines φ = const. are labelled with an increment of 160 gpm. Chart XI represents a composite chart in space valid for the same date and time. It involves the 300 mb analysis in the neighbourhood of the point of departure (New York) and the 200 mb analysis near destination (Amsterdam). Over the ocean 200, 250 and 300 mb data have been consulted. Where two wind data have been plotted one of them refers to the 300 mb level and the other (dotted) to the 200 mb level. The stream lines have been derived by adjusting both 200 and 300 mb analysis and applying some smoothing, together with an inspection of the upper air data at all three levels over the ocean. The spacing of the resulting χ-lines is again 160 gpm, starting from an arbitrary initial value. Finally chart XII shows a composite chart in space and time applying a 300 mb analysis at 12.00 GMT near point of departure and a 200 mb analysis at 18.00 GMT near destination. Over the ocean 200, 250 and 300 mb upper air data for both upper air times have been examined. The isopleths $\mathfrak{z}$ = constant again have been drawn by adjusting both analyses and applying some smoothing, while the spacing again amounts to 160 gpm.

The single heading flight tracks shown, have been constructed by means of the addition method, but the details of the superposition method have not been represented here.

From a consideration of these charts it is obvious that the single heading tracks rather show a minor deviation from each other at the final stage of the flight, where the wind pattern changes rapidly, caused by the fast moving trough to the east.

7. Altimetry determination

After the radio-radar altimeter was brought into operational use during the second world war (1939–1945), the combination with a pressure altimeter made it possible to measure horizontal pressure gradients which enabled the navigator to estimate the geostrophic wind.

The pressure gradient is directly related to the component of wind at right angles to the track by means of the geostrophic relation and the navigator is thus provided with a method to evaluate one component of the drift. By means of a pressure line of position (P.L.O.P. line) the location of the aircraft is facilitated. To determine the drift the navigator must know the true height of the plane and thus, due to the limitations of the use of the radio-radar altimeter, this method is mainly applicable in flights over the sea.

The method of drift determination by altimetry has been described elsewhere (e.g. Sawyer [1949]). We may notice that the results quoted there, may be presented by observing that a small portion of the flight may be interpreted as a "differential" single heading flight. To clarify this point we consider fig. 15, where PQ represents a small portion of the flight track, $\mathbf{c}$ is the true air speed vector and $\mathbf{v}_g$ the (geostrophic) wind vector. If we assume that along PQ the air speed $\mathbf{c}$ remains constant the flight may be considered as being a small single heading flight. In a constant pressure surface we then may write down the

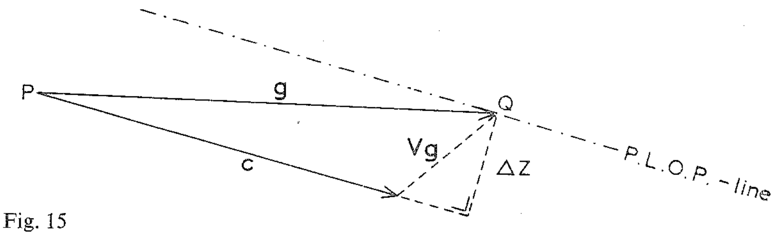

Fig. 15

vertical component of the drift at once from consideration of equation (IV.5).
The displacement $\triangle$ Z becomes

$$\triangle Z = \frac{1}{\lambda} \frac{\varphi(Q) - \varphi(P)}{c}.$$

For quasi-horizontal flights the equation is usually quoted in the form

$$\triangle Z = \kappa \frac{D_2 - D_1}{c}, \qquad \kappa = \frac{g}{\lambda},$$

where D_1 and D_2 represent the "altimeter correction" defined earlier (cf. IV.4). When D is expressed in feet, c in knots, the displacement in n.m. becomes

$$\triangle Z = \frac{21.47}{\sin L_m} \frac{D_2 - D_1}{c}. \qquad \text{(IV.26)}$$

This expression is commonly used in long range transoceanic flights with piston-engined aircraft.

In virtue of the results in subsection 6.2. this expression should be interpreted with some caution. Its validity depends on the condition that the actual pressure-temperature distribution along the track corresponds to that in the standard (I.C.A.N.) atmosphere. When the distribution deviates appreciably from standard conditions and the flight is not quasi-horizontal, then an additional term appears in the expression for the lateral drift $\triangle$ Z. This may be seen from the results for single heading flights in arbitrary surfaces.

Applying formula (IV.10) the displacement $\triangle$ Z becomes

$$\triangle Z = \frac{1}{\lambda} \frac{\varphi(Q) - \varphi(P) + \int_P^Q RTd \ln p}{c}.$$

In the standard atmosphere we have

$$d \ln p = - \frac{1}{RT_s} \, d\varphi_s = - \frac{g}{RT_s} \, dz_p,$$

where T_s, φ_s and z_p stand for the temperature, geopotential and pressure altitude in the standard atmosphere.

Thus, we get

$$\triangle Z = \frac{1}{\lambda} \frac{\varphi(Q) - \varphi(P) - \int_P^Q \frac{T}{T_s} \, d\varphi_s}{c}$$

$$= \frac{1}{\lambda} \frac{\varphi(Q) - \varphi(P) - \varphi_s(Q) + \varphi_s(P) + \int_P^Q \frac{T_s - T}{T_s} \, d\varphi_s}{c}$$

or, on account of (IV.4)

$$\triangle Z = \kappa \frac{D(Q) - D(P) + \int_P^Q \frac{T_s - T}{T_s} \, dz_p.}{c}$$

For simplicity of computation in practice the displacement (n.m.) may be written

$$\boxed{\triangle Z = \frac{21.47}{\sin L_m} \frac{D(Q) - D(P) + \frac{T_s - T}{T_s} \cdot h}{c}} \qquad \text{(IV.27)}$$

where T refers to the mean observed temperature (absolute scale), T_s to the temperature (absolute scale) in the standard atmosphere at the same pressure and h denotes the difference between the readings of the pressure altimeter in the endpoints (feet). The D-values are expressed in feet and the true air speed in knots.

It turns out that the displacement $\triangle Z$ involves an additional term which depends on the temperature excess of the air with respect to standard conditions and the pressure-height difference h between the points where altimeter measurements are made. For quasi-horizontal flights (small h) and approximate standard conditions ($T \simeq T_s$) the additional term may be neglected and the well-known formula (IV.5) be applied. However, in climbing procedures the term may amount to considerable values, by which the navigator has to correct the formula, especially when a continuous cruising climb or stepped cruise is performed.

Table II deals with the correction to be applied to $D_2 - D_1$ (in feet) for various temperature excess values $| T_s - T |$ (°F) for various pressure altitude differences h at selected levels.

TABLE II

pressure altitude of flight level (ft)	h (ft)	$\mid T_s - T \mid$ (°F)				
		10	20	30	40	50
20,000	1,000	20	40	70	90	110
	2,000	50	90	130	180	220
	3,000	70	130	200	270	340
	4,000	90	180	270	360	450
30,000	1,000	20	50	70	100	120
	2,000	50	100	150	190	240
	3,000	70	150	220	290	360
	4,000	100	190	270	390	490
40,000	1,000	30	50	80	100	130
	2,000	50	100	150	200	250
	3,000	80	150	230	300	390
	4,000	100	200	300	400	510

Especially when the temperature excess is high and the climbing procedure is steep, the figures in the table cannot be neglected.

Let us consider a one hour's portion PQ of a flight track of a jet airplane, which contains a step RS of 4,000 ft between 28,000 ft and 32,000 ft pressure altitude (fig. 16). The flight takes place within polar air with a temperature excess of −20° F with respect to the I.C.A.N. atmosphere at 30,000 ft. The true air speed be 470 kn. (D.C.-8).

$$L_m = 55° \text{ N.}$$

Further, let the radio-radar altimeter reading in P be 28,200 ft, in Q 32,800 ft. Then we have

$$D(P) = 28{,}200 - 28{,}000 = 200 \text{ ft},$$

$$D(Q) = 32{,}800 - 32{,}000 = 800 \text{ ft}.$$

$$T_s \ (30{,}000 \text{ ft}) = -48°\text{F}.$$

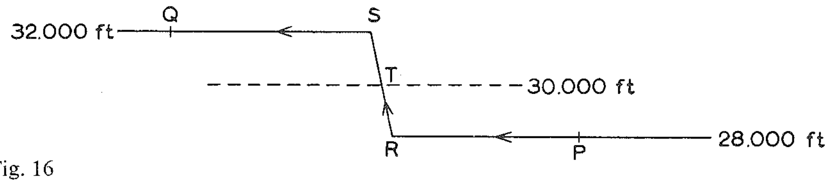

Fig. 16

The displacement ΔZ becomes according to formula (IV.26)

$$\Delta Z = \frac{21.47}{\sin 55°} \cdot \frac{800 - 200}{470} = 26.2 \cdot \frac{600}{470} \sim 34 \text{ n.m.}$$

Entering table II with $| T_s - T | = 20°$F, h = 4,000 ft at 30,000 pressure altitude we find an additional term amounting to 190 ft.

Applying formula (IV.27) we then have

$$\Delta Z = 26.2 \ \frac{600 - 190}{470} \sim 23 \text{ n.m.}$$

The additional term is responsible for a 32% decrease of the displacement.

The displacement formula (IV.27) can still be used for flights with turbo prop and turbo jet powered aircraft in practice, since the available instrumentation aboard of the aircraft makes it possible to determine all quantities needed for computation. The above result however refers to the case that the upper wind may be assumed quasi-stationary. When the wind speed is subject to appreciable changes in time, then the displacement involves another additional term, which depends on the local geopotential tendency. It will be obvious that the computation of ΔZ in practice then partly fails, because it is impossible to determine the local geopotential tendency $\frac{\partial \varphi}{\partial t}$ aboard of the aircraft.

PART V

TRAJECTORY FIELDS

Under certain conditions the trajectories of air particles in non-stationary air flow may be arranged in velocity fields, which may be described by scalar point functions.

In two dimensions the stream function and velocity potential receive consideration. In three dimensions only a velocity potential must be examined. When the actual non-stationary velocity field itself is defined by a scalar point function we may investigate what conditions the scalar point function must satisfy in order that the trajectories may be assembled in *trajectory fields* with a scalar point function. In three dimensions there is only one combination of velocity fields and trajectory fields, both determined by a velocity potential. In two dimensions at least four combinations exist. In the present part the combination in three dimensions and two combinations in two dimensions are investigated. The conditions which the stream function or velocity potential must satisfy offer some atmospheric models, which may be applied in dynamic forecasting by numerical and graphical methods.

1. On the classification of velocity fields and trajectories

In the classification of two-dimensional non-stationary horizontal velocity fields we are concerned with three types, namely the velocity field with a stream function, characterized by

$$\nabla \cdot \mathbf{v} = 0, \mathbf{v} = -\mathbf{k} \wedge \nabla \psi. \tag{V.1}$$

Further, the velocity field with a velocity potential defined by

$$\nabla \wedge \mathbf{v} = 0, \mathbf{v} = -\nabla \varphi \tag{V.2}$$

and finally the Laplacian velocity fields, for which

$$\nabla \cdot \mathbf{v} = 0, \ \nabla \wedge \mathbf{v} = 0,$$
$$\mathbf{v} = -\nabla \varphi = -\mathbf{k} \wedge \nabla \psi.$$

Here the stream function ψ and velocity potential φ are harmonic functions, satisfying Laplace's equation

$$\triangle \psi = \triangle \varphi = 0. \tag{V.3}$$

In space, where we limit our classification to those velocity fields which may be described by *one* scalar point function, there is only one velocity field to be considered, i.e. the *lamellar* velocity field for which

$$\nabla \wedge \mathbf{v} = 0, \quad \mathbf{v} = - \nabla \varphi$$

φ again being a velocity potential.

In our investigation it is of importance to consider those scalar point functions ψ and φ, which involve an additional time variable t.

We have seen, that in meteorology the geostrophic flow in isobaric and other physical surfaces may be interpreted as a velocity field with stream function.

Studying the trajectories of particles which move within the flow, where the velocity distribution is known, we may consider the displacement of an arbitrary chosen field, each point in the field determined by two coordinates (a, b). The coordinates are considered as individually conserved during the motion of the particles, i.e.

$$\frac{da}{dt} = 0, \frac{db}{dt} = 0$$

or

$$\frac{\partial a}{\partial t} = - \mathbf{v} \cdot \nabla a, \quad \frac{\partial b}{\partial t} = - \mathbf{v} \cdot \nabla b.$$

When it is assumed that the particle remains on a specified physical surface, for instance on an isentropic surface, and the wind field is replaced by the geostrophic approximation then the trajectory may suitably be computed by means of electronic computers. Within isobaric surfaces such computations have been performed for the barotropic forecast with the BESK computer (Djuric, Wiin-Nielsen [1957]).

Starting from a set of particles, located at the intersection of a rectangular grid at $t = 0$ the computer determines the location of these points after a certain lapse of time. Rather then give the trajectories themselves the computer yields the final distribution of particles in terms of an arbitrary initial distribution of particles.

If we are interested in the behaviour of the trajectory rather than in successive positions of a set of particles, then the theory of composite topographies with geostrophic flow presents an interesting problem. The problem may be put forward by examination of a theorem for composite charts, outlined in part IV.

It was shown there that any pressure pattern track of an airplane in an isobaric surface could be embedded within a composite topography with geostrophic flow (fig. 7). As a special case we may consider an object which drifts freely with the flow, for instance a constant level balloon, respectively an air particle when it is assumed that the particle remains on the isobaric surface during its motion. With this specification we may state that each trajectory of a particle may be embedded within a composite topography with geostrophic flow. The particle's trajectory is identical with one of the stream lines in the composite topography and the particle's speed is inversely proportional to the distance of the trajectory to adjacent streamlines.

Now we may put the question under what conditions *all* the streamlines of the composite topography represent trajectories of the flow. Then the trajectories are assembled in a "*trajectory field*", which is described by a stream function (fig. 17). The isochrones determine the successive positions of the particles which at t = 0 were located at the initial isochrone t_0.

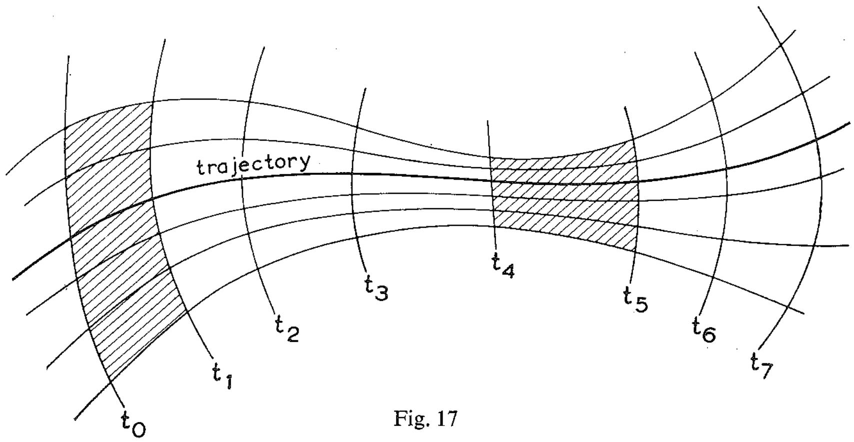

Fig. 17

It is not necessary to claim a stream function for the trajectory field. A trajectory field may alternatively be defined by a velocity potential. Then the trajectories are orthogonal curves of the potential lines.

Returning to the general velocity fields classified above, the problem is to find the conditions whereby the trajectories of particles which move in these fields may be assembled in trajectory fields.

2. Trajectory fields with stream function in velocity fields with stream function

Suppose we have to deal with a velocity field with stream function ψ, then a set of trajectories constitutes a trajectory field if the time function $t = t(x, y)$ satisfies two conditions. First it should define a composite velocity field with stream function. Then according to (II.2) t must be a solution of the partial differential equation

$$J\left(t, \frac{\partial \psi}{\partial t}\right) = 0.$$

Secondly the time function must determine a propagation of isochrones for which the speed of propagation is related to the velocity of the particles by the vector equation

$$\mathbf{v} \cdot \nabla t = 1.$$

Together with (V.1) we have

$$\mathbf{v} \cdot \nabla t = -(\mathbf{k} \wedge \nabla \psi) \cdot \nabla t = -\mathbf{k} \cdot \nabla \psi \wedge \nabla t = J(t, \psi) = 1.$$

The two conditions for the time function

$$J(t, \psi) = 1, \quad J\left(t, \frac{\partial \psi}{\partial t}\right) = 0$$

may be written out:

$$\left\{\begin{aligned} &\psi_y \frac{\partial t}{\partial x} - \psi_x \frac{\partial t}{\partial y} = 1, \\ &\psi_{ty} \frac{\partial t}{\partial x} - \psi_{tx} \frac{\partial t}{\partial y} = 0. \end{aligned}\right. \tag{V.4}$$

It turns out that the time function must be a solution of a system of two quasi-linear partial differential equations. The characteristic determinant of the system (V.4) is

$$J = \begin{vmatrix} \psi_y & -\psi_x \\ \psi_{ty} & -\psi_{tx} \end{vmatrix} = J\left(\psi, \frac{\partial \psi}{\partial t}\right).$$

When the determinant J does not vanish in a certain area, Cramér's method yields

$$\frac{\partial t}{\partial x} = -\frac{\psi_{tx}}{J} = f_1(x, y, t)$$

$$\frac{\partial t}{\partial y} = -\frac{\psi_{ty}}{J} = f_2(x, y, t).$$

When f_1 and f_2 are continuously differentiable in a certain area, then a simultaneous solution $t(x, y)$ of the system (V.4), must fulfill the condition

$$\frac{\partial^2 t}{\partial x \partial y} = \frac{\partial^2 t}{\partial y \partial x}$$

or

$$f_{1y} + f_{1t}f_2 = f_{2x} + f_{2t}f_1. \tag{V.5}$$

When this "integrability condition" does not happen to be an identity, we may solve t from (V.5). If it can be proved in addition that this function $t(x, y)$ satisfies the system (V.4), the time function happens to be a particular solution of the system resulting in an "isolated" trajectory field for the given velocity field.

If however the integrability condition appears to be an identity the system (IV.4) is an involutary system. In that case the system always possesses simultaneous solutions.

The integrability condition (V.5) becomes

$$\frac{-\psi_{yxt}J + \psi_{xt}J_y}{J^2} - \frac{\psi_{yt}}{J}\left(\frac{-\psi_{xtt}J + \psi_{xt}J_t}{J^2}\right)$$

$$\equiv \frac{-\psi_{yxt}J + \psi_{yt}J_x}{J^2} - \frac{\psi_{xt}}{J}\left(\frac{-\psi_{ytt}J + \psi_{yt}J_t}{J^2}\right)$$

or

$$\psi_{xt}J_y + \psi_{yt}\psi_{xtt} \equiv \psi_{yt}J_x + \psi_{xt}\psi_{ytt}$$

or

$$\psi_{xt}(J_y - \psi_{tty}) - \psi_{yt}(J_x - \psi_{ttx}) \equiv 0.$$

This may be written by means of the Jacobian determinant

$$J(\psi_t, J(\psi, \psi_t) - \psi_{tt}) \equiv 0.$$

Considering the rate of change of ψ_t

$$\frac{d}{dt}\psi_t = \psi_{tt} + \mathbf{v}\cdot\nabla\psi_t = \psi_{tt} - (\mathbf{k}\wedge\nabla\psi)\cdot\nabla\psi_t = \psi_{tt} - \mathbf{k}\cdot\nabla\psi\wedge\nabla\psi_t$$

or

$$\frac{d}{dt}\psi_t = \psi_{tt} - J(\psi, \psi_t) \tag{V.6}$$

the integrability condition finally takes the form

$$\boxed{J\left(\psi_t, \frac{d}{dt}\psi_t\right) \equiv 0.} \tag{V.7}$$

This is a partial differential equation of the third order for ψ.

We thus find the result that trajectory fields with a stream function may be found in velocity fields with stream function ψ if ψ statisfies the partial differential equation (V.7).

The condition expresses geometrically that at each moment the tendency curves $\psi_t =$ constant coincide with the curves $\frac{d}{dt}\psi_t =$ constant. In the field of flow, defined by a solution ψ of (V.7) *the pattern of lines of equal tendency is advected geostrophically, eventually accompanied by a change of the tendency value along the lines.*

In order to specify the stream function χ for the trajectory field we have to solve the system of equations (V.4).

Let us consider the second equation of this system. A solution $t = t_o(x, y)$ gives a composite stream function $\psi(x, y, t_o(x, y))$ with associated velocity field with stream function χ.

According to (II.4), $t_o(x, y)$ is determined by the equation

$$\frac{\partial\psi}{\partial t} = -\frac{d\psi^*}{dt}, \tag{V.8}$$

where ψ^* is an arbitrary function of t. The associated stream function χ is, cf. (II.6):

$$\chi = (\psi + \psi^*)_{t_o(x,y)} \tag{V.9}$$

Here $(\ )_{t_o(x,y)}$ denotes a substitution of $t_o(x, y)$ in the expression within parenthesis, as before.

In order that the velocity field for the composite stream function be a trajectory field the auxiliary function ψ^* has to be specified in such a manner that $t_0(x, y)$ also satisfies the first equation of system (V.4).

For that purpose we differentiate (V.8) with respect to x and y

$$\psi_{tt} \frac{\partial t}{\partial x} + \psi_{tx} = - \psi^*_{tt} \frac{\partial t}{\partial x},$$

$$\psi_{tt} \frac{\partial t}{\partial y} + \psi_{ty} = - \psi^*_{tt} \frac{\partial t}{\partial y}.$$

Solving for $\frac{\partial t}{\partial x}$ and $\frac{\partial t}{\partial y}$ and substituting in the first equation of system (V.4) gives

$$\psi_x \psi_{ty} - \psi_y \psi_{tx} = \psi_{tt} + \psi^*_{tt}$$

or

$$J(\psi, \psi_t) - \psi_{tt} = \psi^*_{tt}$$

or

$$\frac{d}{dt} \psi_t = - \psi^*_{tt}.$$

But the original velocity field was characterized by the condition (V.7). From that condition we derive

$$\frac{d}{dt} \psi_t = - F(-\psi_t, t) = - F(\psi^*_t, t)$$

where F is a special function, uniquely determined by the actual velocity field.

Hence ψ^* is determined by the ordinary differential equation

$$\psi^*_{tt} = F(\psi^*_t, t), \tag{V.10}$$

which may be solved by a simple quadrature. ψ^* being specified, $t_0(x, y)$ is known from (V.8) and the stream function χ for the trajectory field follows from (V.9).

Summarizing results we find

Velocity fields with a stream function ψ for which trajectory fields with a stream function χ exist must satisfy the condition $J\left(\psi_t, \frac{d}{dt} \psi_t\right) \equiv 0$.

The time functions for the trajectory fields are simultaneous solutions of the system of equations.

$$J(t, \psi_t) = 0 \quad J(t, \psi) = 1.$$

The stream function χ *associated with the trajectory fields is determined by*

$$\chi = (\psi + \psi^*)_t,$$

where ψ^* *is a solution of the ordinary differential equation*

$$\psi^*_{tt} = F(\psi^*_t, t),$$

F being a special function of ψ_t^* *and t determined by* $J\left(\psi_t, \frac{d}{dt}\psi_t\right) = 0$ *and t being the time function determined by the equation*

$$\psi_t = -\psi_t^*$$

It is worth noticing that the particles in a trajectory field which are located on an isochronal pass equal areas in equal times. This is a consequence of the property that in the trajectory field the product of speed and cross section is constant along a stream filament (fig. 17).

We will demonstrate the theory by an analytic example. Let

$$\psi = Uy - \frac{Lv_0}{2\pi} \sin \frac{2\pi}{L}(x - ct) \tag{V.11}$$

represent the stream function of a sinussoidal velocity perturbation superimposed on a uniform zonal flow U (fig. 18). Then the velocity vector **v** has components

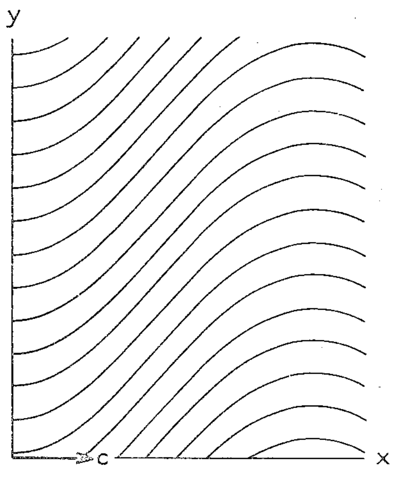

Fig. 18

$$\mathbf{v} = \left(U, v_o \cos \frac{2\pi}{L} (x - ct) \right)$$

The velocity field represents a periodic disturbance having wavelength L, amplitude v_o and velocity of propagation c.

We have first to prove that the velocity field satisfies condition (V.7). For that purpose we compute the individual rate of change of the tendency ψ_t.

Then according to (V.6)

$$\frac{d}{dt} \psi_t = \psi_{tt} - \psi_x \psi_{ty} + \psi_y \psi_{tx}$$

$$\psi_x = -v_o \cos \frac{2\pi}{L} (x - ct),$$

$$\psi_y = U,$$

$$\psi_t = v_o c \cos \frac{2\pi}{L} (x - ct),$$

$$\psi_{tx} = \frac{-2\pi v_o c}{L} \sin \frac{2\pi}{L} (x - ct),$$

$$\psi_{ty} = 0,$$

$$\psi_{tt} = \frac{2\pi v_o c^2}{L} \sin \frac{2\pi}{L} (x - ct).$$

Thus

$$\frac{d}{dt} \psi_t = \frac{2\pi v_o c(c - U)}{L} \sin \frac{2\pi}{L} (x - ct)$$

or

$$\frac{d}{dt} \psi_t = \frac{2\pi(c - U)}{L} (v_o c^2 - (\psi_t)^2).^{\frac{1}{2}} \qquad \text{(V.12)}$$

expressing that $\frac{d}{dt} \psi_t$ is a function of ψ_t i.e. that ψ indeed fulfils condition (V.7). The sinussodial velocity field therefore possesses trajectory fields. To compute the stream function χ we observe that according to (V.12)

$$F = \frac{2\pi(U - c)}{L} (v_o c^2 - (\psi_t)^2)^{\frac{1}{2}}.$$

Then the auxiliary function ψ^* is determined by (V.10)

$$\psi_{tt}^* = \frac{2\pi(U - c)}{L} (v_o c^2 - (\psi_t^*)^2)^{\frac{1}{2}},$$

whence by integration

$$\psi_t^* = v_o c \cos \frac{2\pi}{L} (c - U)(t - t_o),$$

t_o being an integration constant
or

$$-\psi_t^* = v_o c \cos\left(\frac{2\pi}{L}(U-c)t + A\right), \qquad \text{(V.13)}$$

where

$$A = \frac{\pi(1 + 2(U-c)t_o)}{L}.$$

Integration of (V.13) yields

$$\psi^* = \frac{-v_o cL}{2\pi(U-c)} \sin\left(\frac{2\pi}{L}(U-c)t + A\right) + B.$$

B denoting a new integration constant.

The time function for the trajectory fields is determined by the equation (V.8), i.e.

$$v_o c \cos\left(\frac{2\pi}{L}(U-c)t + A\right) = v_o c \cos\frac{2\pi}{L}(x - ct),$$

from which follows

$$t = \frac{x}{U} - \frac{LA}{2\pi U}.$$

Finally the stream function χ becomes on account of (V.9) (apart from an immaterial constant B)

$$\chi = Uy - \frac{Lv_o}{2\pi}\sin\left(\frac{2\pi}{L}\left(\frac{U-c}{U}\right)x + \frac{c}{U}A\right) - \frac{v_o cL}{2\pi(U-c)}\sin\left(\frac{2\pi}{L}\left(\frac{U-c}{U}\right)x + \frac{c}{U}A\right)$$

With $C = \frac{c}{U}A$ we have

$$\chi = Uy - \frac{Lv_o}{2\pi}\frac{U}{U-c}\sin\left(\frac{2\pi}{L}\left(\frac{U-c}{U}\right)x + C\right).$$

Comparing this result, where χ = constant represent trajectories, with the original stream function ψ, we observe that the trajectories of the trajectory fields are all sinussoidal. The amplitude $v_{tr.}$ and the wavelength $L_{tr.}$ are related to the amplitude v_o and wavelength L of the original streamlines according to

$$\frac{v_{tr.}}{v_o} = \frac{L_{tr.}}{L} = \frac{U}{U-c}$$

Thus, when the pattern of sinussoidal streamlines is given and c known, the trajectory fields can be found by using a *scale factor* $\frac{U}{U-c}$ in the streamline pattern. By varying A all trajectory fields are found.

We may remark that any velocity field consisting of an arbitrary velocity perturbation superimposed on a uniform zonal flow U involves trajectory fields.
Here the stream function is

$$\psi = Uy + F(x, t).$$

It may be easily shown that this stream function satisfies condition (V.7).

The differential equation (V.7) for ψ involves two particular solutions.
A. $\psi_t \equiv 0$. The velocity field is stationary. The trajectories coincide with the streamlines and it is evident that trajectory fields may be found, since the trajectory fields are identical with the streamline pattern.

B. $\frac{d}{dt}\psi_t \equiv 0$. These velocity fields are characterized by the property that each particle conserves the tendency ψ_t.
Here

$$F = 0,$$

Thus (V.10) becomes

$$\psi^*_{tt} = 0$$
$$\psi^*_t = a$$
$$\psi^* = at + b, \text{ a and b constant.}$$

Then according to (V.9) the stream function χ associated with a trajectory field assumes the form

$$\chi = (\psi + at)_{t(x,y)} \qquad \text{(V.14)}$$

(where the constant b has been omitted).
The time function is determined by (V.8)

$$\frac{\partial \psi}{\partial t} = -a.$$

When $a = 0$ we have to deal with a *special trajectory field consisting of the enveloping streamlines and isochronals, which coincide with the zero tendency lines.*

The above sinussoidal perturbated zonal flow belongs to the class of velocity fields $\frac{d}{dt}\psi_t \equiv 0$, if $c = U$.
Then

$$\psi = Uy - \frac{Lv_o}{2\pi} \sin \frac{2\pi}{L}(x - Ut),$$

$$\psi_t = v_o U \cos \frac{2\pi}{L} (x - Ut).$$

From $\dfrac{\partial \psi}{\partial t} = -a$ we derive

$t = \dfrac{U}{x} + C$, C being a constant depending on a.

The stream function χ becomes on account of (V.14)

$$\chi = Uy + \frac{a}{U} x + \text{const.}$$

The trajectory fields consist of parallel straight lines, inclined with respect to the x-direction. The special case $(a = 0)$ of the trajectory field which involves the enveloping streamline pattern consists of the set of lines parallel to the x-axis.

3. Trajectory fields with a velocity potential in velocity fields with a velocity potential

Starting from a two-dimensional velocity field with velocity potential we may investigate the condition which the velocity potential must satisfy in order that the trajectories may be taken together in trajectory fields with a velocity potential. To find an answer to this problem we consider it in three dimensions, because the two-dimensional problem may be derived from it. Besides, the problem in three dimensions is more attractive inasmuch as the velocity potential is the only scalar point function to be claimed for the trajectory fields.

Let the three-dimensional velocity field possess the velocity potential φ

$$\mathbf{v} = - \nabla \varphi, \quad \nabla \wedge \mathbf{v} = 0, \tag{V.15}$$

where φ involves, apart from the coördinates x, y and z, the variable t.

$$\varphi = \varphi(x, y, z, t).$$

For a trajectory field to possess a velocity potential it is necessary that it consist of a composite velocity field with velocity potential. The composite velocity field is determined by a time function $t = t(x, y, z)$ which has to be specified in such a manner that the composite velocity field is irrotational.

Similar to the two-dimensional problem for composite velocity fields with a stream function (see part II) it can be shown that the time function must satisfy the condition

$$\nabla t \wedge \nabla \frac{\partial \varphi}{\partial t} = 0,$$

which expresses that t should be a simultaneous solution of three partial differential equations, obtained when the vector equation is written out for its three components. The condition expresses geometrically that the isochronal planes t = const. coincide at each moment t with the planes of equal tendency $\frac{\partial \varphi}{\partial t}$.

In order that the composite velocity field with velocity potential should be a trajectory field with velocity potential, the time function must be such that the speed of propagation of isochronal planes is related to the velocity of the flow according to

$$\mathbf{v} \cdot \nabla t = - \nabla \varphi \cdot \nabla t = 1.$$

The time function t = t(x, y, z) must therefore satisfy both equations

$$\nabla t \wedge \nabla \frac{\partial \varphi}{\partial t} = 0,$$

$$\nabla t \cdot \nabla \varphi = 1 \tag{V.16}$$

simultaneously. In other words, t must be a simultaneous solution of four (quasi-linear) partial differential equations

$$\left\{\begin{array}{rrrl} & \varphi_{tz}\frac{\partial t}{\partial y} & -\ \varphi_{ty}\frac{\partial t}{\partial z} & = 0 \\ \varphi_{ty}\frac{\partial t}{\partial x} & -\ \varphi_{tx}\frac{\partial t}{\partial y} & & = 0 \\ \varphi_{tz}\frac{\partial t}{\partial x} & & -\ \varphi_{tx}\frac{\partial t}{\partial z} & = 0 \\ -\ \varphi_{x}\frac{\partial t}{\partial x} & -\ \varphi_{y}\frac{\partial t}{\partial y} & -\ \varphi_{z}\frac{\partial t}{\partial z} & = 1 \end{array}\right. \tag{V.17}$$

To investigate this system we introduce another variable $\tau = \tau(x, y, z, t)$ by which the system (V.17) changes into a system of homogeneous differential equations (e.g. Kamke [1944]).

$$\left\{\begin{array}{lllll}
 & \varphi_{tz}\dfrac{\partial\tau}{\partial y} & -\varphi_{ty}\dfrac{\partial\tau}{\partial z} & & =0\\[2ex]
\varphi_{ty}\dfrac{\partial\tau}{\partial x} & -\varphi_{tx}\dfrac{\partial\tau}{\partial y} & & & =0\\[2ex]
\varphi_{tz}\dfrac{\partial\tau}{\partial x} & & -\varphi_{tx}\dfrac{\partial\tau}{\partial z} & & =0\\[2ex]
\varphi_{x}\dfrac{\partial\tau}{\partial x} & +\varphi_{y}\dfrac{\partial\tau}{\partial y} & +\varphi_{r}\dfrac{\partial\tau}{\partial z} & -\dfrac{\partial\tau}{\partial t} & =0
\end{array}\right.$$

Any solution $t = t(x, y, z)$ for the first system yields a solution $\tau = \tau(x, y, z, t)$ for the second system and conversely, any solution $\tau = \tau(x, y, z, t)$ of the second system yields a solution $t = t(x, y, z)$ for the first system.

As the characteristic determinant of the second system is equal to zero, we may solve the system for $\dfrac{\partial\tau}{\partial x}$, $\dfrac{\partial\tau}{\partial y}$, $\dfrac{\partial\tau}{\partial z}$ and $\dfrac{\partial\tau}{\partial t}$.

If $\alpha = \alpha(x, y, z, t)$ denotes an arbitrary function of x, y, z, and t, we get

$$\left\{\begin{aligned}
\frac{\partial\tau}{\partial x} &= \alpha\varphi_{tx} = f_1\\
\frac{\partial\tau}{\partial y} &= \alpha\varphi_{ty} = f_2\\
\frac{\partial\tau}{\partial z} &= \alpha\varphi_{tz} = f_3\\
\frac{\partial\tau}{\partial t} &= \alpha(\varphi_x\varphi_{tx} + \varphi_y\varphi_{ty} + \varphi_z\varphi_{tz})\\
&= \alpha\ \nabla\varphi\cdot\nabla\varphi_t = f_4
\end{aligned}\right.$$

Whether the new system possesses simultaneous solutions or not we must investigate the integrability conditions

$$\frac{\partial f_1}{\partial y} \equiv \frac{\partial f_2}{\partial x},\quad \frac{\partial f_1}{\partial z} \equiv \frac{\partial f_3}{\partial x},\quad \frac{\partial f_2}{\partial z} \equiv \frac{\partial f_3}{\partial y}$$

$$\frac{\partial f_1}{\partial t} \equiv \frac{\partial f_4}{\partial x},\quad \frac{\partial f_2}{\partial t} \equiv \frac{\partial f_4}{\partial y},\quad \frac{\partial f_3}{\partial t} \equiv \frac{\partial f_4}{\partial z}$$

The first three conditions give

$$\alpha_y \varphi_{tx} \equiv \alpha_x \varphi_{ty},$$

$$\alpha_z \varphi_{tx} \equiv \alpha_x \varphi_{tz},$$

$$\alpha_z \varphi_{ty} \equiv \alpha_y \varphi_{tz};$$

in vector notation

$$\nabla \alpha \wedge \nabla \varphi_t \equiv 0. \tag{V.18}$$

The last three conditions yield

$$\alpha_t \varphi_{tx} + \alpha \varphi_{ttx} \equiv \alpha \frac{\partial}{\partial x} (\nabla \varphi \cdot \nabla \varphi_t) + (\nabla \varphi \cdot \nabla \varphi_t) \alpha_x,$$

$$\alpha_t \varphi_{ty} + \alpha \varphi_{tty} \equiv \alpha \frac{\partial}{\partial y} (\nabla \varphi \cdot \nabla \varphi_t) + (\nabla \varphi \cdot \nabla \varphi_t) \alpha_y,$$

$$\alpha_t \varphi_{tz} + \alpha \varphi_{ttz} \equiv \alpha \frac{\partial}{\partial z} (\nabla \varphi \cdot \nabla \varphi_t) + (\nabla \varphi \cdot \nabla \varphi_t) \alpha_z$$

or abbreviated in vector form

$$\alpha_t \nabla \varphi_t + \alpha \nabla \varphi_{tt} \equiv \alpha \nabla (\nabla \varphi \cdot \nabla \varphi_t) + (\nabla \varphi \cdot \nabla \varphi_t) \nabla \alpha.$$

Taking the vector product of both sides with $\nabla \varphi_t$, we get

$$\alpha \nabla \varphi_t \wedge \nabla \varphi_{tt} \equiv \alpha \nabla \varphi_t \wedge \nabla (\nabla \varphi \cdot \nabla \varphi_t) + (\nabla \varphi \cdot \nabla \varphi_t) \nabla \varphi_t \wedge \nabla \alpha.$$

But on account of (V.18) this vector equation assumes the form

$$\nabla \varphi_t \wedge \nabla \varphi_{tt} \equiv \nabla \varphi_t \wedge \nabla (\nabla \varphi \cdot \nabla \varphi_t),$$

$$\nabla \varphi_t \wedge \nabla (\varphi_{tt} - \nabla \varphi \cdot \nabla \varphi_t) \equiv 0.$$

Considering the rate of change of φ_t we have

$$\frac{d}{dt} \varphi_t = \varphi_{tt} + \mathbf{v} \cdot \nabla \varphi_t \equiv \varphi_{tt} - \nabla \varphi \cdot \nabla \varphi_t.$$

Hence the integrability condition reduces to

$$\boxed{\nabla \varphi_t \wedge \nabla \frac{d}{dt} \varphi_t \equiv 0} \tag{V.19}$$

Reviewing the result we find that

trajectory fields with velocity potential exist in velocity fields with velocity potential φ when φ satisfies the condition (V.19).

The condition means geometrically that at any moment the surfaces of equal tendency coincide with the surfaces of equal rate of change of the tendency. In the field of flow, defined by a solution φ of (V.19) the surfaces of equal tendency are advected with the flow, eventually accompanied by a change of the tendency value along the surfaces.

In two dimensions we have only to deal with one of the components of the vector equation (V.19), in other words with the component

$$\mathbf{k} \cdot \nabla \varphi_t \wedge \nabla \frac{d}{dt} \varphi_t \equiv 0.$$

This triple vector product involves a unit vector and two gradient vectors, resulting in the possibility of writing it by means of the Jacobian determinant

$$J\left(\varphi_t, \frac{d}{dt} \varphi_t\right) = 0. \tag{V.20}$$

Thus we have

Trajectory fields with velocity potential exist in two-dimensional velocity fields with velocity potential φ, if φ is a solution of the partial differential equation (V.20).

The stream function associated with the trajectory fields may be found in an analogous way as for trajectory fields with a stream function in velocity fields with a stream function. We merely have to replace the stream function ψ by the velocity potential φ in the equations (V.8), (V.9) and (V.10).

4. Discussion

In the diagram below the solid arrows indicate which combinations of two-dimensional velocity fields and trajectory fields with respect to the classification of velocity fields have been dealt with.

For reasons of symmetry there are still two combinations to be studied, namely that of trajectory fields with a velocity potential in velocity fields with a stream function, and that of trajectory fields with a stream function in velocity fields with a velocity potential. An attempt to investigate the integrability conditions showed that these integrability conditions are fairly complicated.

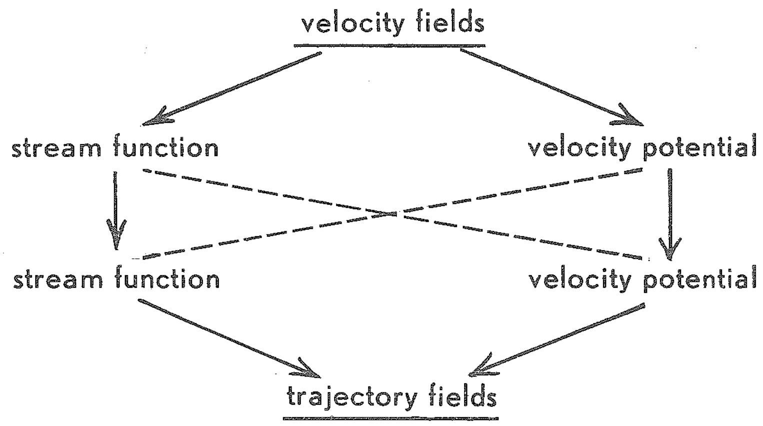

When in addition the velocity fields with both stream function and velocity potential are taken into account the number of combinations increases considerably. Then the stream function ψ and velocity potential φ must be simultaneous solutions of a system of partial differential equations, since ψ and φ already satisfy the Laplace equation.

We may remark that the solution of the problem of trajectory fields within two-dimensional motions of inviscid incompressible fluids already meet with difficulties. By virtue of the equation of continuity such motions may be described by a stream function but in view of the conservation of vorticity in such fluids the stream function must first satisfy the equation

$$\frac{\partial}{\partial t} \triangle \psi + J(\psi, \triangle \psi) = 0.$$

(See Milne–Thomson [1938]).

5. Some models for dynamical forecasting in meteorology

To find some points of contact with the concept of trajectory fields we may call to mind that the upper air flow by means of the geostrophic approximation in isobaric and other physical surfaces may be interpreted as two-dimensional velocity fields with a stream function. It should be stressed that the geostrophic flow applies to the *horizontal projection* of the wind field in the surface under consideration.

Thus, when it is known beforehand that the air particles during their motion do not leave the surface, for instance the isentropic surface, then the theory of trajectory fields only gives some information about the behaviour of the horizontal projection of the trajectories. With this feature in mind, the horizontal projection of trajectories may be arranged in trajectory fields, when the stream function ψ associated with the geostrophic flow in the surface satisfies the equation

$$J\left(\psi_t, \frac{d}{dt}\psi_t\right) = 0. \tag{V.21}$$

For instance, in case of air particles moving upon isobaric surfaces $\left(\frac{dp}{dt} = 0\right)$ the equation reduces to

$$J\left(\varphi_t, \frac{d}{dt}\varphi_t\right) = 0, \tag{V.22}$$

where φ, as before, represents the geopotential.

In case of isentropic surfaces $\left(\frac{d\Theta}{dt} = 0\right)$ we obtain

$$J\left(\psi_M, \frac{d}{dt}\psi_M\right) = 0, \tag{V.23}$$

where ψ_M is Montgomery's stream function.

The equations (V.21), (V.22) and (V.23) are to be interpreted as representing certain atmospheric models . In attempting to simplify the hydrodynamic equations in order to arrive at these models, some rather speculative assumptions are to be made. In this respect the models have no pretensions. They are merely based on the assumption, that the air moves along special physical surfaces with geostrophic wind velocity and that the horizontal projections of the trajectories of the particles may be assembled in trajectory fields.

The models offer the possibility of preparing dynamic forecasts by numerical and graphical methods.

Without going into detail we may remark that the special model for isobaric surfaces

$$\frac{d}{dt}\varphi_t = 0$$

is more or less in agreement with a well-known steering principle, which goes back to Stüve (see for instance Reuter [1954]). This states that the tendency patterns are steered by the quasi-stationary cyclonic and anticyclonic pressure patterns in the direction of the gradient wind.

6. Analysis of a transosonde flight

In part IV it was shown that any pressure pattern track can be embedded in a geostrophic wind configuration, or rather the horizontal projection of the track. When an object is drifting freely with the wind (zero true air speed) the horizontal projection of the trajectory of the object can still be inserted into a geostrophic wind configuration. In a stationary or quasi-stationary air flow the geostrophic wind configuration has to be interpreted as a geostrophic flow in a surface, generated by coinciding isobars, isotherms and isosteric lines. When the object is forced to stay on a physical surface, for instance an isobaric surface, the projection of the trajectory can be embedded within a composite topography of the surface with geostrophic flow. These possibilities occur for balloon flights. The track of a *sounding balloon* for instance can be inserted into a surface with geostrophic flow. The track of a *constant pressure balloon*, where a baroswitch forces the balloon to stay in or near a constant pressure level, can be embedded in a composite topography of the pressure surface with geostrophic flow.

Neiburger and Angell [1956] made a careful analysis of nine flights with constant pressure balloons (C.P.B.) The flights, which lasted several days, were inserted into a number of fixed time upper air analyses which joined each other along straight lines. As a consequence the general view of the flight is somewhat obscured with respect to the upper air flow.

For one of these flights, flight number 996, a composite topography of the 300 mb pressure surface with geostrophic flow was prepared. The balloon was launched in Minneapolis, May 26, 1953. Chart XIII shows the trajectory of the balloon. Two-hour positions derived from a direction finding network are shown by black dots in the centre of circles, the radius of which is an estimate of the fix accuracy. The dots without circles represent estimated or interpolated two-hour positions. Day-time portions of the trajectory are shown by continuous lines, night-time portions by dotted lines. In addition, the locations of two ocean station vessels (station D and E) have been given.

Chart XIV represents the same flight on a larger scale, again with two-hour positions. The drift velocity computed from four-hourly segments is given in knots, by number, above each two-hour position. Radiosonde wind data in the vicinity of the track are shown in conventional fashion. A composite topography with geostrophic flow was prepared by using the published portions of fixed time upper air charts. The stream line $\chi = 0$ determines the trajectory of the C.P.B. balloon. The lines $\chi = 40$, 80, -40 and -80 gpm are adjacent stream lines. The velocity of the balloon corresponds to the geostrophic wind in the χ-pattern. The broken lines represent isochrones-issallo contour lines. The composite chart demonstrates clearly the behaviour of the balloon's motion. At first the balloon drifts within a strong westerly wind, afterwards it shoots along a jetstream until it reaches an upper trough. It passes the axis of the trough and arrives in a considerably weaker south to southwesterly current. The speed of the eastward moving trough is, however, much greater than the eastward component of the balloon's speed. As a consequence the trough overtakes the balloon and the balloon gets upstream of the trough again, where in the meantime the winds have decreased.

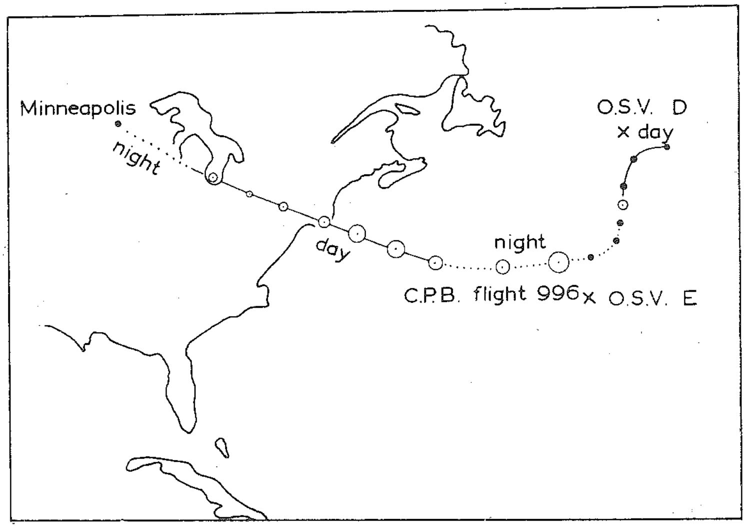

CHART XIII. Constant pressure balloon flight no. 996, starting 26 May 1953, 07.00 G.M.T. from Minneapolis. Dotted portions night-time track, solid portions day-time track. Black dots denote two-hourly positions. Radii of circles give estimate of fix accuracy. Dots without circles are interpolated or extrapolated positions. Positions of ocean station vessels are shown by a cross.

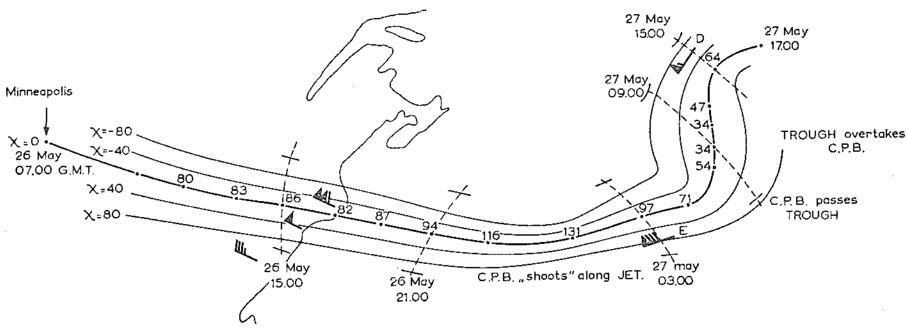

CHART XIV. Same flight on a larger scale. Solid line represents track of C.P.B. with two-hourly positions. Numbers above positions denote balloon's speed in knots. Radiosonde wind data are shown in conventional fashion. Thin continuous lines represent stream lines χ = constant in the composite topography with geostrophic flow (increment 40 gpm). Broken lines represent isochrones – issallo contour lines with line elements copied from original fixed time 300 mb analysis.

REFERENCES

BELLAMY, J. C., 1943
Drift determination with radio and pressure altimeters.
Univ. of Chicago, Inst. of Meteorology (mimeographed).

BIJVOET, H. C., 1956
Over het ontstaan van zware stormen aan de achterzijde van depressies, inzonderheid op de Noordzee.
Meteorologisch Rapport stormvloed 1 Febr. 1953, 2e vervolg (preliminary report; final report to be published elsewhere).

DJURIĆ, DUSAN and AKSEL WIIN-NIELSEN, 1957
Preliminary report on computation of trajectories by means of electronic computers.
Ber. des Deutschen Wetterdienstes, **38**, 22–24.

VAN DER HAM, C. J., 1953
Meteorologisch Rapport stormvloed 1 Februari 1953.
K.N.M.I. (preliminary report; final report to be published elsewhere).

DE JONG, H. M., 1956
Theoretical aspects of aeronavigation and its application in aviation meteorology.
K.N.M.I. Med. en Verh., **64.**

KAMKE, E., 1944
Differentialgleichungen. Lösungsmethoden und Lösungen II.
Partielle Differentialgleichungen erster Ordnung für eine gesuchte Funktion.
Becker und Erler, Leipzig.

KOCHANSKY, A., 1958
Ageostrophic deviations and wind prognoses.
Journ. of Met., **15**, 84–90.

MILNE THOMSON, L. M., 1938
Theoretical Hydrodynamics, 107.
Mc Millan and Co., London.

MONTGOMERY, R. B., 1937
A suggested method for representing gradient flow in isentropic surfaces.
Bull. Am. Met. Soc., **18** 210–212.

MURRAY, R., 1954
On the accuracy of contour charts in forecasting upper winds.
Prof. Notes No. 110, Met. Office, London.

NEIBURGER, M., ANGELL, J. K., 1956
Meteorological applications of constant pressure balloon trajectories.
Journ. of Met., Vol. **13**, 166–194.

REITER, E., 1958
The layer of maximum wind.
Journ. of Met., **15**, 27–43.

REUTER, H., 1954
Methoden und Probleme der Wettervorhersage.
Springer Verlag, Wien.

SAWYER, J. S., 1949
Theoretical aspects of pressure pattern flying.
Met. Rep., Vol. **1** no. 3. Met. Off. London.

23, 25, 26, 27, 29*b*, 30, 31, 33, 34*b*, 35, 36, 37, 38, 39, 40, 41, 42, 43, 44, 45, 46, 47, 48.

alsmede:

49. A. Labrijn. Het klimaat van Nederland gedurende de laatste twee en een halve eeuw. — The climate of the Netherlands during the last two and a half centuries. 1945. (114 blz. met 6 fig. en 1 kaart) . . . . f 1,15

50. J. P. M. Woudenberg. Het verband tussen het weer en de opbrengst van wintertarwe in Nederland. — The correlation between weather and yield of wheat in the Netherlands. 1946. (43 blz. met 6 fig.) 0,70

51. S. W. Visser. Weersverwachtingen op langen termijn in Nederland. — Long range weather forecasts in the Netherlands. 1946. (143 blz. met 25 fig.) 2,05

52. R. J. v. d. Linde en J. P. M. Woudenberg. Een methode ter bepaling van de breedte van een schaduw in verband met den tijd van een jaar en de oriëntatie van het beschaduwde object. — A method for determining the daily variation in width of a shadow in connection with the time of the year and the orientation of the overshadowing object. 1946. (6 blz. met 2 fig. en 2 kaarten) 0,40

53. A. Labrijn. Het klimaat van Nederland. Temperatuur, neerslag en wind. — The climate of the Netherlands. Temperature, precipitations and wind. 1946. (71 blz. met 1 kaart) 2,50

54. C. Kramer. Electrische ladingen aan berijpte oppervlakten. — Electric charges on rime-covered surfaces. 1948. (128 blz. met 17 fig. en 1 afb.) 3,00

55. J. J. Post. Statistisch onderzoek naar de samenhang tussen het weer, de grasproductie en de melkaanvoer. — Statistical research on the correlation between the weather, grass production and milk supply. 1949. (119 blz. met 25 fig. en 6 tab.) . . 3,00

56. R. J. v. d. Linde and J. P. M. Woudenberg. On the microclimatic properties of sheltered areas. The oak-coppice sheltered area. — Over de microklimatologische eigenschappen van beschutte gebieden. Het landschap met eikenhakhoutwallen. 1950. (151 blz. met 52 fig.). 3,00

57. C. Kramer, J. J. Post en W. Wilten. Klimaat en brouwgerstteelt in Nederland. — Climate and growing of malting-barley in the Netherlands. 1952. (149 blz. met 27 fig.). 2,25

58. W. van der Bijl. Toepassing van statistische methoden in de klimatologie. — Applications of statistical methods in climatology. 1952. (197 blz. met 19 fig.) . . . 7,60

59. Tien wetenschappelijke bijdragen, uitgegeven bij het 100-jarig bestaan van het K.N.M.I. — English summary, 1954. (198 blz. met 53 fig.) 12,50

60. C. Kramer, J. J. Post en J. P. M. Woudenberg. Nauwkeurigheid en betrouwbaarheid van temperatuur- en vochtigheidsbepalingen in buitenlucht met behulp van kwikthermometers. 1954. (60 blz. met 11 fig.) 3.50

62. C. Levert. Regens. Een statistische studie. 1954. (246 blz. met 67 fig. en 143 tab.) 10,00

63. P. Groen. On the behaviour of gravity waves in a turbulent medium, with application to the decay and apparent period increase of swell 1,50

64. H. M. de Jong. Theoretical aspects of aeronavigation and its application in aviation meteorology 4,50

65. J. G. J. Scholte. On seismic waves in a spherical earth 5,00

66. G. Verploegh. The equivalent velocities for the Beaufort estimates of the wind force at sea. 1956. (38 blz. met 17 tab.). 1,75

67. G. Verploegh. Klimatologische gegevens van de Nederlandse lichtschepen over de periode 1910—1940. Dl. I: Stormstatistieken. — Climatological data of the Netherlands light-vessels over the period 1910—1940. P. I: Statistics of gales. 1956. (68 blz. met tabellen) . . . . f 3,50

68. F. H. Schmidt. On the diffusion of stack gases in the atmosphere. 1957. (60 blz., 12 fign. en tabn.) 5,00

69. H. P. Berlage. Fluctations of the general atmospheric circulation of more than one year; their nature and prognostic value. 1957 7,50

70. C. Kramer. Berekening van de gemiddelde grootte van de verdamping voor verschillende delen van Nederland volgens de methode van Penman. 1957. (85 blz., fig. en tab.). 7,00

71. H. C. Bijvoet. A new overlay for the determination of the surface wind over sea from surface weather charts. 1957. (35 blz., fig. en tab.) 2,50

72. J. G. J. Scholte. Rayleigh waves in isotropic and anisotropic elastic media. 1958. (43 blz., fig. en tab.) . . . . 3,—

73. M. P. H. Weenink, A theory and method of calculation of wind effects on sea levels in a partly enclosed sea, with special application to the southern coast of the North sea (112 blz., fig. en tab.). . . . . f 8,00

924644* - 140